UNIVERSIDADE DE LISBOA
FACULDADE DE CIÊNCIAS
DEPARTAMENTO DE FÍSICA

Synchronization of Physical Oscillators

Sara Isabel Aleixo Perestrelo

Mestrado em Física

Especialização em Física da Matéria Condensada e Nanomateriais

Dissertação orientada por:
Professor André Moitinho de Almeida
Professor Henrique M. Oliveira

2018

Acknowledgments

A special thanks to my advisor, Henrique Oliveira, and, most of all, to Fred.

Abstract

The phenomenon of synchronization can be found in several biological and non-biological systems, such as, for example, in physical pendulum clocks, metronomes, pacemaker cells, firefly interaction and planet orbits. In this work we present a study concerning the synchronization of two coupled pendulum clocks. We use techniques of Dynamical Systems, in particular, when we study the Andronov model for an oscillator with impulses.

We study the cases for a frequency relation of $1:1$. We analyze the amplitude of the limit cycles of each oscillator and find an asymptotic stable fixed point for the velocity of an isolated clock. In a study of the phase, we construct the functions that map the phase difference between two coupled clocks and analyze its evolution, for a frequency relation of $1:1$. We do the same study for a frequency relation of $2:1$, which is a a study made by the first time in this work. We find one stable fixed point and one unstable fixed point, both for frequency relations of $1:1$ and $2:1$. We conclude that the system of coupled Andronov clocks tend to synchronize in phase opposition for the case $1:1$ and in generalized phase opposition for the case $2:1$.

Also, we make a construction by phase approximation for the first order of the linear expansion, for frequency relations of $N:1$. We then expand in second order the maps for a frequency relation of $1:1$. With this approach, the results coincide with the more complicated technique of studying the original model, this technique is more suitable for numerical studies.

Under the conditions of our problem, we conjecture that we have a *master-slave* relation for a frequency relation of $N:1$, for $N>1$, based on the observations of the maps of the phase difference and on the analysis of the linear expansions.

We construct the regions of synchronization in the parameter space – the Arnold tongues – for two coupled Andronov clocks with frequency relations of $1:1$, $2:1$ and $3:1$. We also analyze what effect does the friction have in these synchronization regions, which, in the synchronization of two Andronov clocks, is a new observation.

Finally, we study the amplitude again, but now we do not assume the occurrence of phase locking. The orbits of the unperturbed system of coupled clocks can be described in the $\mathbb{R}^2$ surface of an invariant torus in phase space. We introduce the a Kolmogorov-Arnold-Moser like theory to verify that under a small limited perturbation to the system, the structure of the torus surface remains stable, which is, again, a new approach for the Andronov model.

Keywords: Huygens, Synchronization, Oscillator, Andronov, torus.

Resumo

O fenómeno da sincronização pode ser encontrado em diversos sistemas na natureza, tal como em relógios de pêndulo, metrónomos, células de pacemaker, interacção entre pirilampos, sistemas planetários, osciladores moleculares, circuitos electrónicos, redes neuronais, como em muitos outros exemplos que são tão estudados como desconhecidos.

Neste trabalho apresentamos um estudo relativamente à sincronização de dois relógios de pêndulo acoplados. Usamos técnicas de Sistemas Dinâmicos, em particular, tendo por base o modelo de Andronov para um oscilador movido a impulsos. Trata-se de um sistema constituído por uma componente oscilatória – no nosso caso, o pêndulo, – e por uma fonte de energia externa periódica – que corresponde ao sistema de engrenagens do pêndulo e que fornece impulsos de energia com uma periodicidade bem conhecida. A particularidade deste tipo de oscilador, que se faz evidenciar principalmente nos capítulos finais deste trabalho, é que a fonte de energia externa é descontínua e a perda de energia ao longo das oscilações é contínua. Esta característica faz com que o sistema seja do tipo *damping and charge*, ao contrário de um sistema do tipo *integrate and fire*, constituído por uma fonte de energia contínua e descargas pontuais, com uma periodicidade bem conhecida, sempre que o sistema atinge um limite de saturação. Existe mais documentação sobre os sistemas de osciladores do tipo integrate and fire. Estes ocorrem frequentemente na natureza e são bem conhecidos. No entanto, um sistema do tipo damping and charge deve estar presente em todos os sistemas acoplados onde se encontre uma entidade geradora de impulsos periódicos com uma intensidade suficiente para ter uma certa influência mínima no sistema. Tal é o caso de pulsares ou cefeidas variáveis, cuja rotação e luminosidade, respectivamente, têm um período bem definido e, como tal, podem servir de força externa periódica para um sistema de osciladores.

No desenvolvimento do nosso trabalho nós nunca damos ênfase às diferenças entre estes dois tipos de sistemas de osciladores, mas deixamos antes a sua categorização para os capítulos finais da dissertação. No desenvolvimento preferimos incidir antes nas características do modelo de Andronov, que se enquadra nos osciladores do tipo damping and charge. Depois de descrever a base do modelo de Andronov para um oscilador com impulsos, nós iniciamos a descrição do sistema de um relógio isolado, revendo conceitos e resultados já conhecidos e que servem de referência para o nosso trabalho. De seguida estudamos dois relógios de pêndulo acoplados, e aqui descrevemos as condições inerentes à aplicabilidade do modelo de Andronov ao caso de interesse. Também aqui revemos resultados anteriores, mas fulcralmente apresentamos novos resultados. Nos capítulos finais do trabalho a categorização dos diferentes tipos de sistemas de osciladores, tanto do tipo damping and charge, como integrate and fire é revista, mas não de forma exaustiva. Alguns exemplos conhecidos e documentados são apresentados, tanto para um caso como para outro.

Iniciamos o estudo do sistema de um relógio de pêndulo isolado, e cumprimento com as condições estabelecidas pelo modelo de Andronov. Fazemos uma análise da estabilidade deste sistema. Para o caso particular do sistema de dois relógios de pêndulo acoplados, incidimos no estudo para uma relação de frequências de $1:1$ Primeiramente, fazemos uma análise da amplitude dos ciclos limite de cada oscilador e encontramos um ponto fixo assimptoticamente estável para a velocidade de um relógio isolado – o isolamento a que nos referimos em todo este trabalho prende-se com o facto de o relógio não sentir qualquer interacção exterior, perdendo apenas energia ao longo do ciclo devido ao atrito seco. Aqui consideramos que a resistência do ar, um tipo de atrito fluido, é desprezável: para além da sua intensidade ser residual em comparação com a intensidade do atrito seco, também a sua presença nas equações do movimento não permitiriam os resultados obtidos a nível da estabilidade do sistema. Já o atrito seco, representado por um valor constante, tem uma influência preponderante no sistema e permite um manuseamento mais simples das equações do movimento.

Quando fazemos o estudo da fase, construímos as funções que mapeiam a diferença de fase entre dois relógios de pêndulo acoplados e analisamos a sua evolução, para relações de frequências de $1:1$ e $2:1$. Encontramos um ponto fixo estável, de valor $\phi_f^s = \pi + \arcsin\left(\frac{\pi h^2 \delta}{8\alpha\mu}\right)$ e um ponto fixo instável, de valor $\phi_f^u = -\arcsin\left(\frac{\pi h^2 \delta}{8\alpha\mu}\right)$ para o caso $1:1$. Para o caso $2:1$ encontramos um ponto fixo estável,

de valor $\phi_f^s = \pi + \arcsin\left(\frac{\pi h^2 \delta}{2\alpha\mu}\right)$, e um ponto fixo instável, de valor $\phi_f^u = -\arcsin\left(\frac{\pi h^2 \delta}{2\alpha\mu}\right)$. Quando o parâmetro ϵ, que expressa a diferença de velocidades (parâmetro de dessintonização), $\omega_2 = \omega_1 + \epsilon$, é muito pequeno, então, tanto para o caso $1:1$ como para o caso $2:1$ observamos que os pontos fixos são $\phi_f^s \approx \pi$ e $\phi_f^u \approx 0$. Daqui, concluímos que o sistema de dois relógios de Andronov acoplados tendem a sincronizar em oposição de fase. Este resultado foi observado graficamente para relações de frequências até $10:1$.

Para além do mais, numa outra secção, fazemos uma construção por aproximação de fase para a primeira ordem da expansão linear, para as relações de frequência de $N:1$. Seguidamente, expandimos em segunda ordem a composição de mapas para uma relação de frequência de $1:1$ e verificamos um comportamento concordante relativamente ao mapa não linear original da diferença de fase. O estudo das expansões lineares é de extrema importância pois, uma vez verificada a sua concordância com os mapas da diferença de fase construídos inicialmente, então é preferível trabalhar com as expansões, por uma questão de simplicidade.

Uma vez sob as condições do nosso problema, conjecturamos que temos uma relação de *master-slave* para uma relação de frequências de $N:1$, desde que $N > 1$, tendo em conta as observações feitas dos mapas da diferença de fase e também a análise feita às expansões lineares de primeira ordem. Não demonstramos aqui esta conjectura, mas antes deixamo-la a demonstrar na continuidade e progresso do nosso trabalho.

Depois, através de um método iterativo usado para encontrar pontos de equilíbrio, construímos as regiões de sincronização no espaço dos parâmetros – as línguas de Arnold – para dois relógios de Andronov acoplados com relações de frequência de $1:1$, $2:1$ e $3:1$. Neste caso, o espaço dos parâmetros corresponde ao espaço (ϵ, α), onde ϵ é o parâmetro da dessintonização e α é a intensidade da interacção que medeia a comunicação entre os dois relógios de pêndulo. Uma das análises que fazemos é a comparação das línguas de Arnold conseguidas a partir dos mapas não lineares para a diferença de fase e as respectivas expansões lineares de primeira ordem. Observamos uma concordância notável para o caso $1:1$, concordância esta que se mantém, mas que decresce com o aumento de N. Esta comparação foi feita para $N = 1$, $N = 2$ e $N = 3$.

Outra análise que fazemos é o efeito que o atrito seco tem nestas regiões de sincronização. Concluímos que o atrito seco, sob as condições do problema, contribui para aumentar a área das línguas de Arnold, o que significa que um sistema acoplado deste tipo com um maior amortecimento está mais susceptível de sincronizar depois de um certo número de oscilações. Isto é válido, claro, fora da região de sobreamortecimento, cujo estudo não é do nosso interesse nem é, portanto, desenvolvido nesta tese.

Por fim, voltamos a uma análise da amplitude, mas agora não assumimos, como anteriormente, a ocorrência de *phase locking*. Partimos do princípio que a intensidade da interacção é dependente da diferença de fase entre ambos os relógios. Assim, em lugar de realizarmos uma descrição determinística da evolução da amplitude dos dois ciclos limite, consideramos uma perturbação estocástica. As órbitas do sistema não perturbado de relógios acoplados pode ser descrito na superfície $\mathbb{R}^2$ de um toro invariante no espaço de fases. Nós introduzimos uma variante da teoria de Kolmogorov-Arnold-Moser para verificar que, perante a nova perturbação estocástica no sistema, que assumimos apenas ser pequena e limitada, a estrutura do toro ainda permanece estável. Isto é equivalente a dizer que o sistema é estruturalmente estável. A superfície bidimensional do toro que representa o sistema não perturbado passa então a ser uma superfície difusa tetradimensional, resultado do produto de dois ciclos limite bidimensionais, de cada um dos relógios, agora perturbados. Esta é uma nova abordagem ao modelo de Andronov no que toca à estabilidade do sistema em estudo.

Palavras-Chave: Huygens, Sincronização, Oscilador, Andronov, toro.

List of Figures

Contents

1 Introduction

1.1 Purposes and Goals

In this work we deal with the phenomenon of synchronization [27, 15, 18, 5] of a physical system. This phenomenon occurs when all its constituents adjust their rhythms of self-sustained periodic oscillators due to their weak interaction to operate the system in unison.

A self-sustained oscillator is one that contains an internal source of energy which is converted into an oscillatory movement which in turn continues to generate the same rhythm until the source expires. The communication between both oscillators is governed by a weak interaction which, in the case of this thesis, is based on a periodic pulsed-stimulation.

Synchronization is observed very often in nature, from simple physical clocks [23, 22, 28] and metronomes [5], to firefly communication [21, 18, 29] and electronic oscillators [27]. In all of these systems we can identify oscillators (clocks, fireflies, electronic circuits) that emit a periodic pulse – pulsed oscillators – and a weak interaction (material vibrations, light emitting impulses, electronic pulses).

The phenomenon of synchronization has been studied since the XVII century and was first recorded by Christiaan Huygens in 1656, detailed in a letter he sent to *de Sluse* [17]. Huygens observed that two pendulum clocks in the same wall in the vicinity of each other synchronize in phase opposition, even when slightly perturbed or placed further apart of each other. In this particular system, each pendulum clock receives periodic impulses of energy from their escapement. These impulses propagate through the wall and perturb the movement of its counterpart. Because they slightly perturb each other every cycle, we say they are coupled, and because we have a periodic interaction, we may say that they are "pulsed-oscillators".

As Huygens never got to fully understand the described phenomenon from a physical and mathematical point of view, it is our goal to find out what drives pendulum clocks to synchronize through a detailed description of this physical system. For this purpose, we base our work on the Andronov model for an oscillator with impulses [3]. We review the works done in [24, 22], which in part consist of the application of this model to similar isolated and coupled pendulum clocks. We also develop further work in terms of coupling of clocks with different velocities and study the stability of the system. This model not only describes the pendulum motion, but can also be applied to physical systems of different scales such as large-scale networks, electronic oscillators, molecular oscillators, among many other systems provided with self-sustained oscillators connected by a periodic weak interaction.

We aim to understand the problem of the pendulum clocks from the perspective of Dynamical Systems. Firstly, in subsection 1.2, we review some aspects of phase dynamics, in particular the model of Kuramoto [19]. In subsection 1.3, we introduce some historical notes about the appearance of the pendulum clock. We also describe the gear system of the pendulum clock for a better understanding of the base model behind our system of interest. In subsection 2.1 we study the amplitude of an isolated Andronov oscillator – which we refer as the Andronov clock. In subsection 3.1 we apply the same analysis to two coupled Andronov clocks that share an interaction between them for a frequency relation of $1:1$. Here, we make an analysis of the amplitude of oscillations and then an analysis of the phase. In subsection 3.2, we just analyze the phase evolution, but for a frequency relation of $2:1$. Afterwards, in subsection 4.1 we study the phase evolution of both clocks: we construct linear approximations that map the phase difference between them and find the respective points of stability. This analysis is applied to clocks with frequency relation from $1:1$ to $N:1$ (the fastest clock completes N cycles for one cycle of the slowest clock). In subsection 4.2 we expand in second order the map for the phase difference of two clocks with frequency relation $1:1$ and verify the concordance behavior between the original map. Afterwards, in subsection 4.3, we find the synchronization regions in parameter space. We do this by constructing the Arnold tongues of the system, using the original maps. We also construct the Arnold tongues using the linear expansions of the constructed maps of the phase difference. We compare both constructions for frequency relations $1:1$, $2:1$, $3:1$ and $4:1$. Still in this section, we establish a conjecture about a master-slave relation between both clocks. Finally, in section 5, using Kolmogorov-Arnold-Moser (KAM) theory, we prove analytically that this system is stable under a small and bounded perturbation.

This proof is achieved by showing that the $\mathbb{R}^4$ toroidal surface that outcomes from the product of the two perturbed limit cycles remains in a neighborhood of the unperturbed $\mathbb{R}^2$ original torus.

1.2 Phase Dynamics

In this work we deal with a system of a self-sustained oscillator with a periodic external force. This external force is weak, in the sense that it has an effect so small on the amplitude of the self-sustained oscillator, that we are able to neglect it, considering only the phase dynamics. This approach is based on a perturbation technique based on the phase dynamics approximation, explored by Kuramoto, [19]. Consider a general M-dimensional system

$$\frac{d\mathbf{x}}{dt} = \mathbf{f}(\mathbf{x}), \qquad \mathbf{x} = (x_1, ..., x_M) \in \mathbb{R}^M, \tag{1.1}$$

where f is a function satisfying some regularity properties, like being Lipschitz sectionally continuous.

Now suppose that this system has an attractive periodic solution with period T_0, $\mathbf{x}_0(t) = \mathbf{x}_0(t + T_0)$. In the *phase space* this solution is an isolated closed attractive trajectory, called *limit cycle*. The representative point in the phase space moving along the cycle represents the self-sustained oscillations and it is represented by the angular coordinate, Φ [27]. When the phase growth is uniform, along the movement, it is governed by the equation

$$\frac{d\Phi}{dt} = \omega_0, \tag{1.2}$$

where $\omega_0 = \frac{2\pi}{T_0}$ is the frequency of self-sustained oscillations. The phase of this uniform rotation, Φ, can be always obtained from a nonuniformly rotation of angle θ performed on the cycle through the formula [27]

$$\Phi = \omega_0 \int_0^{\theta} \left[\frac{d\tilde{\theta}}{dt}\right]^{-1} d\tilde{\theta}. \tag{1.3}$$

When such an oscillatory system is perturbed, either by external forces or by other oscillators coupled to it, however weak the force may be, the representative point of phase Φ no longer stays on the limit cycle, but instead, it deviates to a region close to the initial trajectory. This region, which must be close to the limit cycle, is now the object of study, rather than a well defined trajectory, so that the phase approximation dynamics is possible, allowing us to deal solely with the phase of the oscillations. Thus, equation 1.2 is rewritten as

$$\frac{d\Phi}{dt} = \nabla_{\mathbf{x}}(\Phi) \cdot \mathbf{f}(\mathbf{x}) = \omega_0. \tag{1.4}$$

The validity of this model lies in the definition of the perturbed phase: it is now written as $\Phi(\mathbf{x})$, and is called *asymptotic phase*, since it lies on a neighborhood of the original limit cycle. The perturbed motion is then described as

$$\frac{d\mathbf{x}}{dt} = \mathbf{f}(\mathbf{x}) + \beta\, \mathbf{p}(\mathbf{x}, \mathbf{t}), \tag{1.5}$$

where β is a parameter used to indicate the smallness of the perturbation. This smallness must be of such an order that the dynamics of equation 1.5 holds identically to the dynamics of equation 1.1.

Further refinement of this approximation is carried out in [19]. It is also one of the working bases of [27]. Our approach will be based on the Andronov model for an oscillator with impulses, which considers already the phase approximation dynamics, which is intrinsic to the model and a limit cycle for one oscillator, which is constructed sectionally from three linear and Hamiltonian dynamical system. We analyze in detail the synchronizing dynamics for two coupled oscillators.

1.3 Working system of a pendulum clock

In this subsection we give an overview of the working system of the pendulum, as well as some aspects of its history. The essential of this description follows closely chapter 10 of the book *The Pendulum – a case study in physics* [4].

It was by 1637 that Galileo Galilei (1564-1642) realized the possibility of using the pendulum as the central beating mechanism in a clock. In 1641 Galileo and his son, Vincenzio, begun developing a design for a pendulum clock with the central idea of employing a falling weight as a driving force to maintain the oscillations. Galileo never got to finish his work, and the pendulum clock project was left uncompleted by the time of Vincenzo's death, in 1649. It was Christiaan Huygens who resumed the original work of Galileo and developed it to what we may consider the primordial design of the pendulum clock.

In his major work, *Horologium Oscillatorium (The Pendulum Clock or Geometrical Demonstrations Concerning the Motion of Pendulums as Applied to Clocks)*, published in 1673, Huygens projected the new design of a pendulum clock and what distinguished his work from the work of Galileo was the realization of the escapement and its connection to the swinging bob.

(a) Christiaan Huygens (1656–1657)

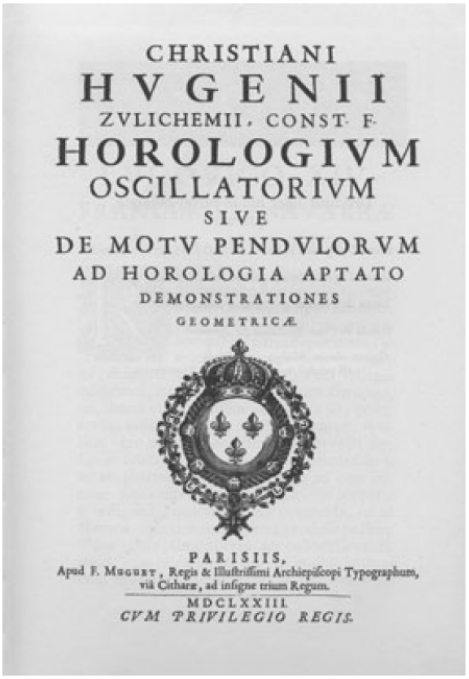

(b) *Horologium Oscillatorium*

Figure 1.1: Christiaan Huygens on the left and, on the right the title page from a facsimile edition of *Horologium Oscillatorium*, his major work on horology (1673).

The basic arrangement for Huygens' pendulum clock escapement is represented in figure 1.2a. The externally driven crown wheel rotates in only one direction, in interrupted intervals paced by the swinging motion of the vertical rod.

As we can see, in parts *I* and *III* of figure 1.2b, the fall of the weight (part *III*) initiates a complex chain of notching movements between the sprockets that result in the rotation of the crown wheel on top of the escapement (part *I*). This rotation makes the pallets of the horizontal verge (that later in 1671 were replaced by an anchor escapement) to notch in the crown wheel every time the pendulum passes through the vertical position, always in the same direction. This notch is responsible for every "click" heard at every cycle of the pendulum. The "click" also corresponds to an impulse of kinetic energy provided by the escapement to the pendulum, allowing it to continue the oscillations.

Huygens observed that two clocks of his invention, suspended in the same wall shared some sort of what he called "sympathy", which we refer in this work as the phenomenon of synchronization (and that is the purpose of our study). As he wrote in a letter [17] on February, 1665,

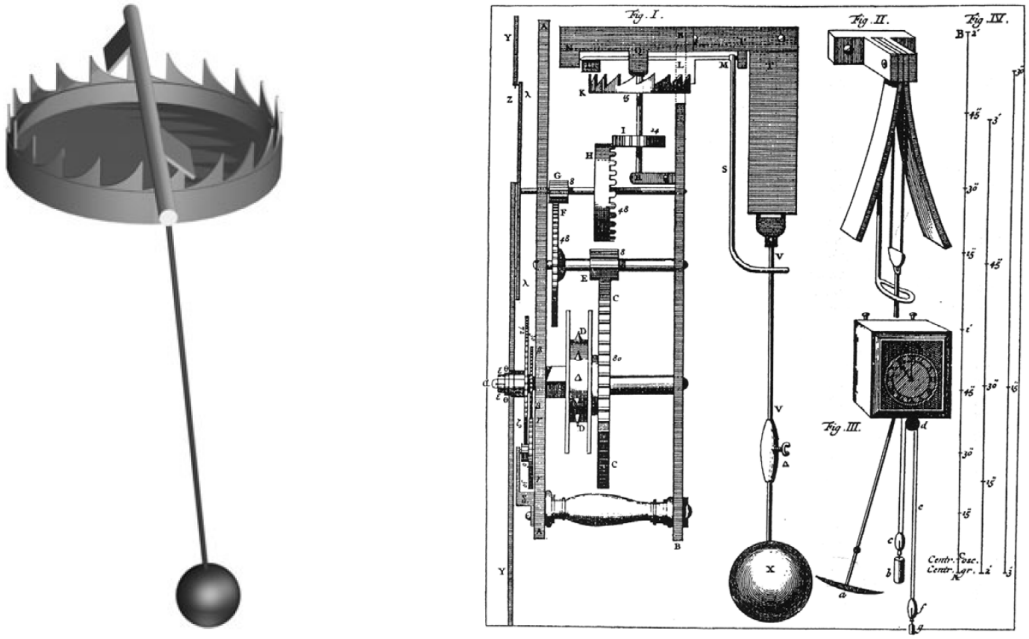

(a) Simplified pendulum mechanism (b) Pendulum design (*Horologium Oscillatorium*)

Figure 1.2: On the left, a simplified scheme of the pendulum mechanism idealized by Huygens and, on the right, an illustration of Huygens' pendulum in his *Horologium Oscillatorium* (1673).

> *"The two clocks, while hanging [on the wall] side by side with a distance of one or two feet between, kept in pace relative to each other with a precision so high that the two pendulums always swung together, and never varied. While I admired this for some time, I finally found that this happened due to a sort of sympathy: when I made the pendulums swing at differing paces, I found that half an hour later, they always returned to synchronism and kept it constantly afterwards, as long as I let them go. Then, I put them further away from one another, hanging one on one side of the room and the other one fifteen feet away. I saw that after one day, there was a difference of five seconds between them and, consequently, their earlier agreement was only due to some sympathy that, in my opinion, cannot be caused by anything other than the imperceptible stirring of the air due to the motion of the pendulums."*

In order to study this phenomenon in more detail, we simplify the escapement of the system, previously described, to the basic necessary features that allow us to translate this mechanical contraption into the Andronov model. The Andronov model for an oscillator with impulses is a mathematical model that describes the motion of an oscillator in the same conditions as the pendulum clock. This model and the conditions for which a reasonable approximation to the physical system holds is described in the next section.

2 Model for an Isolated Physical Oscillator

2.1 The Andronov Model of an Oscillator

The essential ideia of the Andronov model [3] is based on a model of a physical pendulum clock, like the one explained in subsection 1.3. Regardless of the form of the external energy supply – e.g., a weight-driven or a spring-driven pendulum, where is the fall of the weight or the torsion of the spring, respectively, that provides energy to the escapement –, the crown wheel provides an impulse of kinetic energy to the swinging mass every time it passes through the vertical position, just in one direction (e.g., always from right to left), allowing the oscillatory movement to continue.

Of course, to start each cycle, the transferred kinetic energy must be greater than a certain minimum value – we consider this value to be $\frac{h^2}{2}$, which, in this case, is normalized to the mass of the pendulum and h has velocity units. This amount of energy must be greater than the action of the mechanical friction inside the clock, or otherwise the oscillations will not get over the overdamped regime. The total energy of the system in each cycle is conserved by the balance between the energy provided by these impulses and the dissipated energy. The latter is associated to a parameter that we introduce as the dry friction.

So let us translate this system mathematically. A generic equation of the damped harmonic oscillator can be written as

$$\ddot{q} + F(\dot{q}) + \omega^2 \ \sin(q) = 0, \tag{2.1}$$

where q is the generalized angular coordinate and ω is the natural frequency of oscillation.

In the system of the pendulum clock the damping term, $F(\dot{q})$, involves a fluid friction and a dry friction component. The fluid friction is associated to the air resistance to the movement of the pendulum and it is proportional to the velocity, while the dry friction involves the contact between two solid surfaces and, in this case, comes from the action of the gears from the mechanical system that provides the impulses at every cycle and is constant (does not depend on the velocity). We chose to consider only dry friction, because the effect of the air resistance is negligible compared to the former [3], and because it is proportional to the velocity. We consider, therefore, that the friction that acts on this physical system is represented by

$$F(\dot{q}) = \mu \ sign(\dot{q}), \tag{2.2}$$

where μ is the dry friction coefficient and $sign(\dot{q})$ returns 1 or -1, whether $\dot{q} > 0$ or $\dot{q} < 0$, respectively.

The external force is periodic and corresponds to an instantaneous energy supply from the escapement. It consists of a periodic impulse that happens at the starting point of every cycle, $q = q_0 = q(t = 0)$. These impulses occur in a very short period of time, τ, such that $\tau << T$, where T is the period of a complete oscillation. In the rest of each cycle there is no energy supply, such that the clock behaves like a damped harmonic oscillator. It is also known that, for sufficiently small oscillations, $\sin(q) \approx q$, and that is precisely the regime of the pendulum motion. So, the equation that governs the pendulum motion is

$$\ddot{q} + \mu \ sign(\dot{q}) + \omega^2 \ q = 0. \tag{2.3}$$

We see that, for small values of friction, μ, this oscillator is quasilinear, whereas for large μ it is of relaxation type and must be integrated sectionally [27]. In this work, as we will see later in section 3, we obtain the limit cycle using a linear piecewise approach (equation 3.4), which is always exact.

Let us proceed to the dimensional analysis of equation 2.3. For the sake of simplicity and consistency, equation 2.3 is normalized to the mass of the pendulum, therefore, all components must have acceleration units. The functions $sign(x)$ and $\sin(x)$ are dimensionless. In the second component of the equation, $sign(\dot{q})$ does not have units, therefore, μ is treated as a normalized force ($\frac{1}{s^2}$) – the force of friction –, although it was initially presented as a simple coefficient as a measure of the dissipation of the system. This is consistent with the model formulated by Andronov, in [3].

In short, the main assumptions made by this model are the following:

1. The impulse received by the pendulum is instantaneous and acts as the pendulum passes the equilibrium position, in just one direction (e.g., always from right to left);

2. The pendulum receives the same amount of kinetic energy, $\Delta K = \frac{h^2}{2}$ (normalized to the mass of the pendulum), after each oscillation;

3. The friction is independent of the angular velocity (dry friction, associated to the contact between the gears in the internal mechanism of the clock).

Note that, by assumptions 1 – an instantaneous impulse – and 2 – only kinetic energy –, the impulse affects exclusively the velocity of the pendulum. The instant at which the impulse acts and its magnitude are entirely determined by the position and the state of the pendulum, respectively. This implies that the system is autonomous.

Particularizing equation 2.3 for different signs of the velocity, we get two branches:

$$\begin{cases} \ddot{q} + \mu \ + \omega^2 \, q = 0, & \dot{q} \geq 0 \\ \ddot{q} - \mu \ + \omega^2 \, q = 0, & \dot{q} < 0 \end{cases}, \tag{2.4}$$

and with a suitable change of variables,

$$\begin{cases} x_1 = q + \frac{\mu}{\omega^2} \\ x_2 = q - \frac{\mu}{\omega^2} \end{cases}, \tag{2.5}$$

we get two simple harmonic oscillator equations,

$$\begin{cases} \ddot{x_1} + \omega^2 \, x_1 = 0, & \dot{x_1} \geq 0 \\ \ddot{x_2} + \omega^2 \, x_2 = 0, & \dot{x_2} < 0 \end{cases}, \tag{2.6}$$

whose solutions are a parametrization of two distinct circles, centered in $-\frac{\mu}{\omega^2}$ and in $\frac{\mu}{\omega^2}$, respectively:

$$\begin{cases} q_i(t) = A_i \, sin(\omega t) + B_i \, cos(\omega t) = -\frac{\mu}{\omega^2} \\ q_j(t) = A_j \, sin(\omega t) + B_j \, cos(\omega t) = \frac{\mu}{\omega^2} \end{cases}. \tag{2.7}$$

We use the solutions above to construct a curve, as shown in figure 2.1, so that the index i denotes values corresponding to the upper half of the phase plane and the index j denotes values corresponding to the lower half. In order to represent the movement of the pendulum as a continuous trajectory in the two-dimensional phase space, the Andronov model misaligns the center of the upper and lower circles by a distance of $2\,\frac{\mu}{\omega^2}$, which is equivalent to establish the conditions $q_i(t) = q_j(t)$ and $\dot{q}_i(t) = \dot{q}_j(t)$ at the critical positions $(q, \dot{q}) = (q_{max}, 0)$ and $(q, \dot{q}) = (-q_{max}, 0)$, respectively. This guarantees the continuity of the movement, as shown in figure 2.2.

Figure 2.2 shows the phase portrait of the system, which is a limit cycle with initial conditions conveniently established to be $q(t = 0) = -\mu/\omega^2$ and $\dot{q}(t = 0) = v_0$. It is here, in this starting point of the cycle, where a quantity of kinetic energy, $\Delta K = \frac{h^2}{2}$, is transferred from the escapement of the clock to the pendulum.

The effect of the friction is represented by the radius decrease, however, it is constant along the quarters 1 and 3 and along the lower half-circle. Due to this decrease, the action of the impulses is represented by the noticeable discontinuity on top of the cycle, in the vertical semi-axis of the velocity.

The dry friction is associated to a constant loss of energy, which is directly related to a constant radius decrease in a cycle. From equation 2.7, where q_k, A_k and B_k are, respectively, the angular coordinate and the amplitudes in the region k ($j = 1, 3$, $i = 2$) of the limit cycle 2.2, and the initial conditions, we can calculate this decrease. At $t = 0$, the velocity and position are

$$\begin{cases} q_1(0) = B_1 - \frac{\mu}{\omega^2} = -\frac{\mu}{\omega^2} \\ \dot{q}_1(0) = \omega A_1 = v_0 \end{cases} \Leftrightarrow \begin{cases} B_1 = 0 \\ A_1 = \frac{v_0}{\omega} \end{cases} \tag{2.8}$$

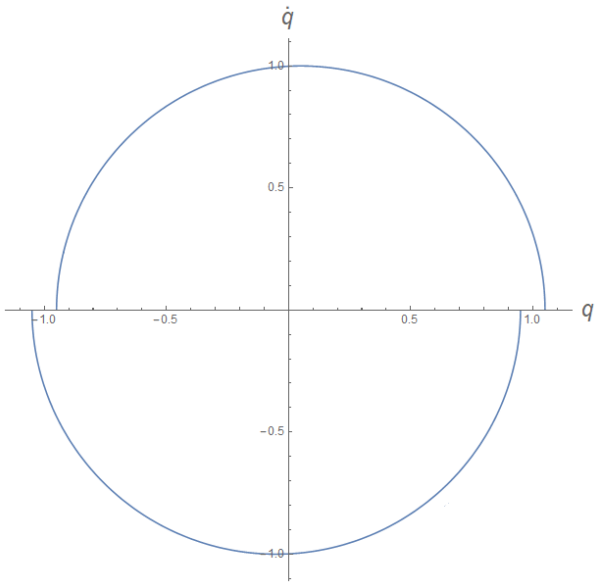

Figure 2.1: Two semi-circles of same radius, but with different centers, which are solutions of equations 2.7. The values chosen for the intervening parameters are $\mu = 0.05$, $\omega = 1$. Here in the figure the shift is highly exaggerated when compared to the values of the performed simulations.

We establish a condition that guarantees the continuity of the movement at the critical positions $(q, \dot{q}) = (q_{max}, 0)$ and $(q, \dot{q}) = (-q_{max}, 0)$. In order to maintain the consistency with the radius decrease along the limit cycle, the semi-axes must be misaligned. Under these conditions, at $t = \frac{\pi}{2\omega}$ we have:

$$\begin{cases} q_1(\frac{\pi}{2\omega}) = q_2(\frac{\pi}{2\omega}) \\ \dot{q}_1(\frac{\pi}{2\omega}) = \dot{q}_2(\frac{\pi}{2\omega}) = 0 \end{cases} \Leftrightarrow \begin{cases} A_2 = A_1 - 2\frac{\mu}{\omega^2} \\ \dot{q}_{1,2}(\frac{\pi}{2\omega}) = 0 \end{cases} . \tag{2.9}$$

At $t = \frac{3\pi}{2\omega}$ we have:

$$\begin{cases} q_2(\frac{3\pi}{2\omega}) = q_3(\frac{3\pi}{2\omega}) \\ \dot{q}_2(\frac{3\pi}{2\omega}) = \dot{q}_3(\frac{3\pi}{2\omega}) = 0 \end{cases} \Leftrightarrow \begin{cases} A_3 = A_2 - 2\frac{\mu}{\omega^2} \\ \dot{q}_{2,3}(\frac{3\pi}{2\omega}) = 0 \end{cases} . \tag{2.10}$$

Since the amplitude A_3 remains constant until $t = \frac{2\pi}{\omega}$, we can say that the loss in the amplitude after a whole cycle is

$$A_3 - A_1 = -4\frac{\mu}{\omega^2}. \tag{2.11}$$

and, consequently, knowing from 2.8 that the amplitude has the form of $A = \frac{v}{\omega}$, we get the loss in velocity:

$$\frac{v_f}{\omega} - \frac{v_0}{\omega} = -4\frac{\mu}{\omega^2} \Leftrightarrow v_f - v_0 = -4\frac{\mu}{\omega} \tag{2.12}$$

where $v_f = \omega A_3$ is the final velocity after a whole cycle.

One of the main goals of this work is to translate this dynamical system into a function that predicts the behavior of a cycle based on the previous one. This is possible tracing a Poincaré section [14] at the semi-axis $q = -\mu/\omega^2$ and $\dot{q} > 0$. We now introduce the notation symbols "$-$" and "$+$" to represent the instants immediately before and after the impulse is given, respectively. The balance of kinetic energy at the Poincaré section gives

$$K_{n+1}^{+} = K_n^{-} + \Delta K, \qquad \Delta K = h^2/2, \tag{2.13}$$

where ΔK is the impulse of kinetic energy, normalized to the mass of the pendulum, which is provided by the escapement. From equation 2.13, we have

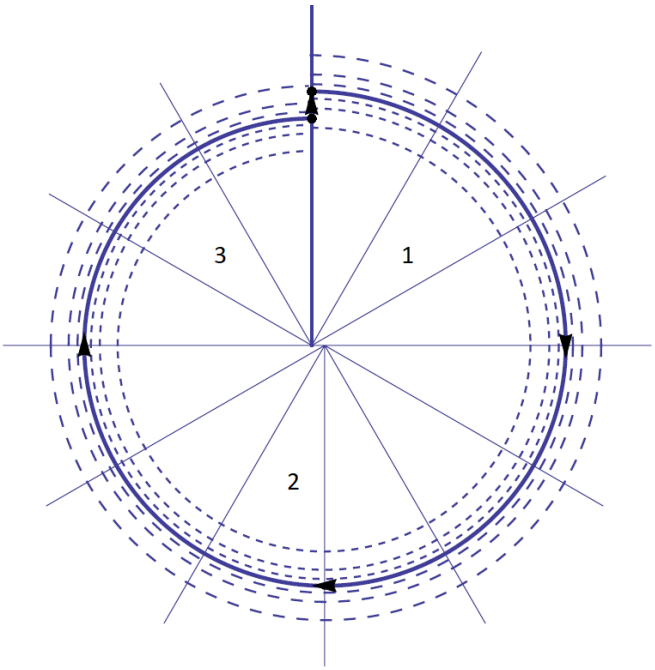

Figure 2.2: Limit cycle of an isolated clock represented as a solid curve in the phase space. Horizontal axis represents the angular position and in the vertical axis the velocity. We use normalized coordinates to get arcs of circles 1, 2 and 3.

$$\frac{1}{2}\,(v_{n+1}^{+})^2 = \frac{1}{2}\,(v_n^{-})^2 + \frac{1}{2}\,h^2. \tag{2.14}$$

but, by equation 2.12, if we consider $v_0 = v^+$ and $v_f = v^-$ as the velocities at the beginning and at the end of the n-th cycle, respectively, we get $v_n^- = v_n^+ - 4\frac{\mu}{\omega^2}$. And so, from equation 2.13, the velocity of the $(n+1)$-th cycle can be written as

$$v_{n+1}^{+} = \sqrt{(v_n^+ - 4\mu/\omega)^2 + h^2}. \tag{2.15}$$

The notation can be simplified by dropping the superscript "+", since it refers to the velocity at the initial point of the limit cycle. We write

$$v_{n+1} = \sqrt{(v_n - 4\mu/\omega)^2 + h^2}, \tag{2.16}$$

The equation above defines a Poincaré map, which is a function $P : \Sigma \to \Sigma$, such that $x_{n+1} = P(x_n)$. The hypersurface Σ is transversal to the flow in the (N-dimensional) phase space and has $N-1$ dimensions [14]. The main advantage of the Poincaré section is that the points corresponding to flow trajectories are mapped one to another by means of a simpler function, therefore providing a more clearly vision of the original flow.

To find the points of stability of the system – that imply periodic trajectories or closed orbits – we take equation 2.16, in the form $f(v_{n+1}) = v_n$, and consider the fixed point condition $f(v^*) = v^*$. We find the fixed point:

$$v^* = \frac{A^2 + h^2}{2A}, \qquad A = 4\mu/\omega, \tag{2.17}$$

where A is the friction component.

Figure 2.3 shows that the vertical segment of the bold line marks the threshold between the over-damped and the oscillation regimes. The intersection of the bold curve with the diagonal reveals a fixed point. Now the main interest is to know whether this fixed point is stable or unstable. In particular, we

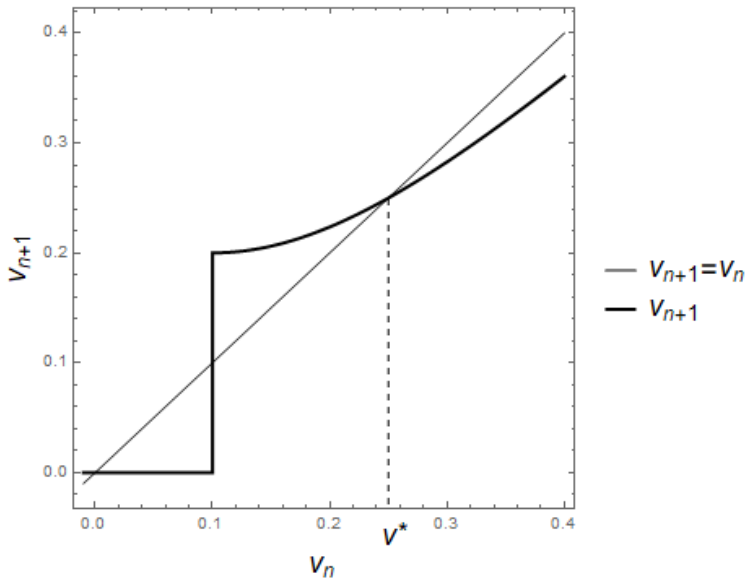

Figure 2.3: Plot of v_{n+1} *vs* v_n at the Poincaré section (bold). The straight line indicates all the possible fixed points of the system, as long as they intercept the line of the dynamical system, at $v^* \approx 0.25$. Note that the intersection of the vertical line does not belong to the dynamics, marking, in fact, the threshold between the overdamped and damped regimes of oscillations, at $v_n = h = 0.1$.

are interested in asymptotic stability, *i.e.*, an *attractive* fixed point. An attractive fixed point is a point v^* such that for every point v_n in a sufficiently small neighborhood, the iterated function sequence

$$v_n, P(v_n), P(P(v_n)), P(P(P(v_n))), ... \tag{2.18}$$

converges to v^*.

In this case, the stability condition is given by $|P'(v^*)| < 1$. A point v^* that holds said condition is an attractive fixed point. The latter is directly associated to an attractive closed orbit, therefore the neighboring trajectories converge to a periodic one. In fact, the derivative at every point is given by

$$\left|\frac{dP(v_n)}{dv_n}\right| = \frac{v_n - A}{\sqrt{(v_n - A)^2 + h^2}}, \tag{2.19}$$

which is always $< 1 \; \forall \; v_n > A + h$, hence v^* is an attractive fixed point and therefore it represents an attractive closed orbit.

3 System of Two Coupled Pendulum Clocks

3.1 A 1:1 Frequency Relation

In this section we follow [23]. By analyzing the velocity, we verified that the pendulum clock viewed as a dynamical system is stable in its amplitude of oscillations, since the iterations of the respective Poincaré map converge to a stable equilibrium point. Now, in this section we are considering the effect of a weak interaction that results from the coupling of two pendulum clocks. This interaction is small in the sense that it influences only the phase of each oscillator. This means that we can describe the dynamics of the system with a phase equation (in the case of coupled clocks, since we always take one of the clocks as reference, we deal with *phase difference* equations). In section 5 we will establish conditions to the validity of this model, that is, the meaning of the word "small" in this context.

Consider two coupled pendulum clocks, clock 1 and clock 2, attached to a rigid beam. When clock 1 passes through the vertical position, the energy of the received impulse is propagated through the beam, generating a perturbation α in the movement of the clock 2 and vice-versa [23],[1]. It is assumed that this perturbation:

1. has units of velocity and therefore acts exclusively on the vertical component of the limit cycle;
2. is much smaller than the friction component, i.e., $\alpha << A$ (defined in equation 2.16);
3. is constant;
4. corresponds to a kick always in the same direction.

The assumptions 3 and 4 lead to a downward displacement of the limit cycle by α, as it is shown in figure 3.1. The changes to equation 2.3 are such that the perturbation is determined by the position of the clock j, but its intensity is felt by clock i.

$$\ddot{q}_i + \mu_i \; sign(\dot{q}_i) + \omega_i^2 \; q_i = -\alpha_i F(t), \tag{3.1}$$

where $i, j = 1, 2$; $i \neq j$ and $F(t) = \delta(t - t_j)$ is a Dirac Delta distribution, that locates the perturbation at the time instant t_j at which the impulse of the clock j takes place. The set of time instants $\{t_j\}_{i=1,\ldots,N}$ denote every time the clock j passes by the vertical position, of coordinates $(q, \dot{q}) = (-\frac{\mu}{\omega^2}, v_{max})$ in the phase space. Further on we will see, in this subsection and in subsection 3.2 that these time instants are calculated along the description of the limit cycle, although we do not explicit its important here in equation 3.1.

Analogously to the equation 2.3, in a dimensional analysis we deal with acceleration units. Unlike the dry friction coefficient, μ, which denotes an acceleration, the constant α expresses the instantaneous variation of the velocity on the vertical axis, without changing the position of the oscillator. It denotes a simple difference in velocities, thus, it has velocity units (s^{-1}). This is consistent with equation 3.3, which must have a dimensionless argument, as we will see further on. Necessarily, $F(t)$, has velocity units as well. In fact, the Dirac Delta distribution is the result of deriving a Heaviside function, $\Theta(t)$, to be more precise for this case, a function that expresses an instantaneous change in velocity. Therefore, the Dirac Delta distribution acquires the inverse units of the units of its arguments. Thus, $F(t)$ carries on velocity units (s^{-1}). The complete second member of the equation is, therefore, an acceleration, consistently ($s^{-1} \times s^{-1} = s^{-2}$).

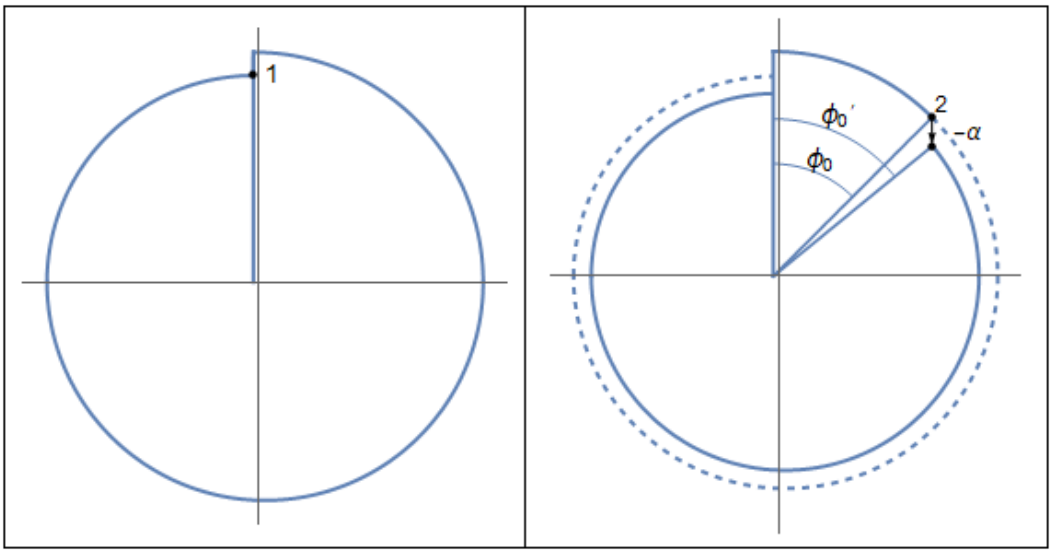

Figure 3.1: Limit cycles of clocks 1 and 2, at left and right, respectively. The passage of the clock 1 by the equilibrium position perturbs the movement of the clock 2, causing a decrease in the velocity of its limit cycle.

When plotting the Poincaré map we see that a positive value of α decreases the energy of the system and shifts the fixed point v^* to the left,

$$v^* = \frac{(A + \alpha)^2 + h^2}{2(A + \alpha)}, \qquad A = 4\mu/\omega, \tag{3.2}$$

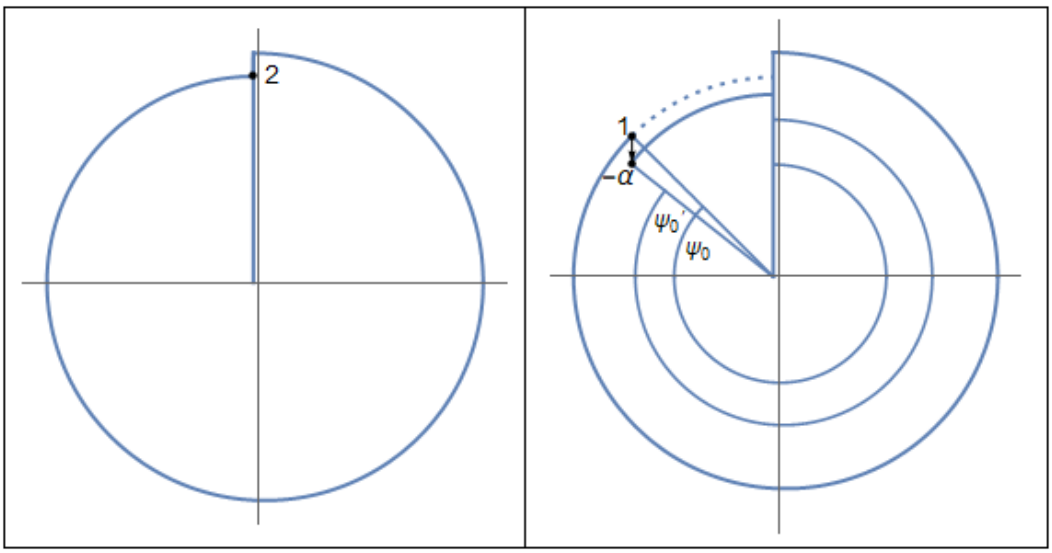

Figure 3.2: Limit cycles of clocks 2 and 1, at left and right, respectively. Now the passage of the clock 2 by the equilibrium position decreases the velocity of the limit cycle of clock 1.

as shown in figure 3.3. But despite the effect of the perturbation, the dynamics remain almost the same, as evidenced by the previous formula, and as we'll see in section 5.

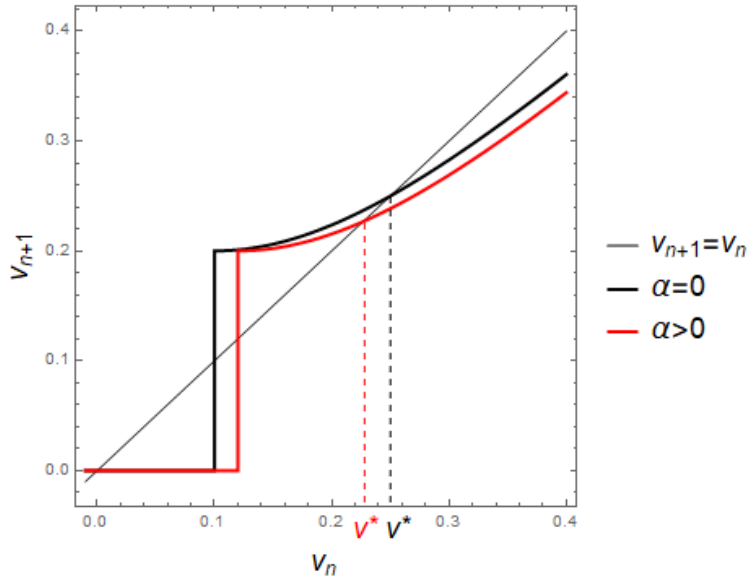

Figure 3.3: Perturbed (red) and non perturbed (black) system. The fixed point v^* shifts with the value of the perturbation α.

Intuitively, by figures 3.1 and 3.2, it seems that over the cycles the clocks tend to depart from each other until the distance between them reaches its maximum, that is, a phase difference of π. Based on this intuition, the goal now is to analyze the phase difference between clocks 1 ($C1$) and 2 ($C2$) at the beginning and at the end of one cycle. For this purpose, a few important notes must be considered:

1. Time is measured by the reference clock, $C1$ and, for the sake of convenience, it is considered that the clocks do not overtake each other.

2. Three important time instants must be taken in consideration: t_0, t_1 and t_2, before $(-)$ and after $(+)$ the impulse of energy. Instants t_0^+ and t_2^- mark the beginning and the end of one cycle;

3. $C1$ and $C2$ have frequencies $\omega_1 = \omega$ and $\omega_2 = \omega + \epsilon$, respectively, with $\epsilon << \omega$.

At t_0^-, $C1$ is at the vertical position (at initial coordinates of the phase space) with phase 0 while $C2$ has phase ϕ_0. The phase difference is ϕ_0. At t_0^+, $C1$ receives an impulse and the generated perturbation affects $C2$'s phase such that $\phi_0 \rightarrow \phi_0' = \sigma(\phi_0, \omega_2, \alpha)$, where σ is a function that maps old phase values to phase-perturbed ones by the following expression:

$$\sigma(\phi_i, \omega_i, \alpha_i) = \arctan\left(\sin(\phi_i), \cos(\phi_i) - \frac{\alpha_i}{\gamma(\phi_i, \omega_i)}\right), \quad i = 1, 2. \tag{3.3}$$

where ϕ_i and ω_i are the phase and velocity of the clock i that is affected by the impulse, respectively. The effect of the map $\sigma(\phi, \omega, \alpha)$ is to decrease by the amount $\frac{\alpha}{\gamma(\phi,\omega)}$ the velocity at the phase ϕ, without changing the position. The function γ expresses the amplitude of the limit cycle all around itself, by sections. Therefore it denotes, a velocity, which makes the argument of the function 3.3 dimensionless, and it is defined as

$$\gamma(\phi, \omega) = \begin{cases} \frac{h^2\omega}{8\mu} + \frac{2\mu}{\omega}, & 0 \leq \phi < \frac{\pi}{2}, \\ \frac{h^2\omega}{8\mu}, & \frac{\pi}{2} \leq \phi < \frac{3\pi}{2}, \\ \frac{h^2\omega}{8\mu} - \frac{2\mu}{\omega}, & \frac{3\pi}{2} \leq \phi < 2\pi, \end{cases} \tag{3.4}$$

By the analysis of function $\gamma(\phi, \omega)$, we can see that the loss of velocity is, once again, $\gamma(2\pi, \omega) - \gamma(0, \omega) = -\frac{4\mu}{\omega}$, consistently to the analysis made in section 2.1. An observation is that, because

$$\gamma\left(0 \leq \phi < \frac{\pi}{2},\, \omega\right) > \gamma\left(\frac{\pi}{2} \leq \phi < \frac{3\pi}{2},\, \omega\right) > \gamma\left(\frac{3\pi}{2} \leq \phi < 2\pi,\, \omega\right), \tag{3.5}$$

we have that

$$\sigma\left(0 \leq \phi < \frac{\pi}{2},\, \omega,\, \alpha\right) < \sigma\left(\frac{\pi}{2} \leq \phi < \frac{3\pi}{2},\, \omega,\, \alpha\right) < \sigma\left(\frac{3\pi}{2} \leq \phi < 2\pi,\, \omega,\, \alpha\right), \tag{3.6}$$

which means that the higher is the value of the velocity, the lower is the effect of the perturbation felt.

The time $C2$ takes to reach the vertical position is $\Delta t_{C2} = \frac{2\pi - \phi_0'}{\omega_2}$. At t_1^-, the phases of $C2$ and $C1$ are, respectively:

$$\begin{cases} \Phi_2(t_1^-) = 2\pi \\ \Phi_1(t_1^-) = \varphi_0 \end{cases} \tag{3.7}$$

However, after the impulse, at t_1^+, the change to Φ_1 is $\varphi_0 \rightarrow \varphi_0' = \Delta t_{C2}\, \omega_1$, so the new phases at t_1^+ are:

$$\begin{cases} \Phi_2(t_1^+) = 2\pi \\ \Phi_1(t_1^+) = (2\pi - \sigma(\phi_0, \omega_2, \alpha))\frac{\omega_1}{\omega_2} \end{cases} \tag{3.8}$$

So, the time $C1$ takes to reach the vertical position again is given by $\Delta t_{C1} = \frac{2\pi - \varphi_0'}{\omega_1}$. Therefore, when $C1$ reaches the point right before the energy impulse, at t_2^-, the phases of $C1$ and $C2$ are, respectively:

$$\begin{cases} \Phi_1(t_2^-) = 2\pi \\ \Phi_2(t_2^-) = 2\pi + \Delta t_{C1}\, \omega_2 \end{cases} \tag{3.9}$$

The phase difference between both clocks, seen that $\Phi_2(t_0^+) - \Phi_1(t_0^+) = \phi_0 - 0 = \phi_0$ at the beginning

of the cycle, is now given by:

$$\begin{aligned}\phi_1 &= \Phi_2(t_2^-) - \Phi_1(t_2^-)\\ &= (2\pi + \Delta t_{C1}\,\omega_2) - 2\pi =\\ &= (2\pi - \varphi_0')\frac{\omega_2}{\omega_1} =\\ &= (2\pi - \sigma(\varphi_0, \omega_1, \alpha))\frac{\omega_2}{\omega_1} =\\ &= \left(2\pi - \sigma\Big((2\pi - \sigma(\phi_0, \omega_2, \alpha))\,\frac{\omega_1}{\omega_2}, \omega_1, \alpha\Big)\right)\frac{\omega_2}{\omega_1}.\end{aligned} \tag{3.10}$$

To simplify the previous equation, we use the function $r(x, d) = (2\pi - x)d$, with coefficients $d_1 = \frac{\omega_1}{\omega_2}$ and $d_2 = \frac{1}{d_1}$, to write the phase difference between both clocks ϕ_1 as a composition of four maps. Note that the function r maps values of the phase of a clock after the other clock performs a path towards the vertical position, while the map σ is just a kick action on a clock:

$$\phi_1 = r(\sigma(r(\sigma(\phi_0, \omega_2, \alpha), d_1), \omega_1, \alpha), d_2). \tag{3.11}$$

Applying this combination to the $(n+1)$-th cycle, the previous equation can be written as follows:

$$\phi_{n+1} = \Omega_{1:1}(\phi_n), \tag{3.12}$$

where Ω is the composition of four maps that relate the phase difference of clocks $C1$ and $C2$ in the $(n+1)$-th cycle in terms of the n-th cycle. The dynamics related to the phase difference is shown in figure 5.

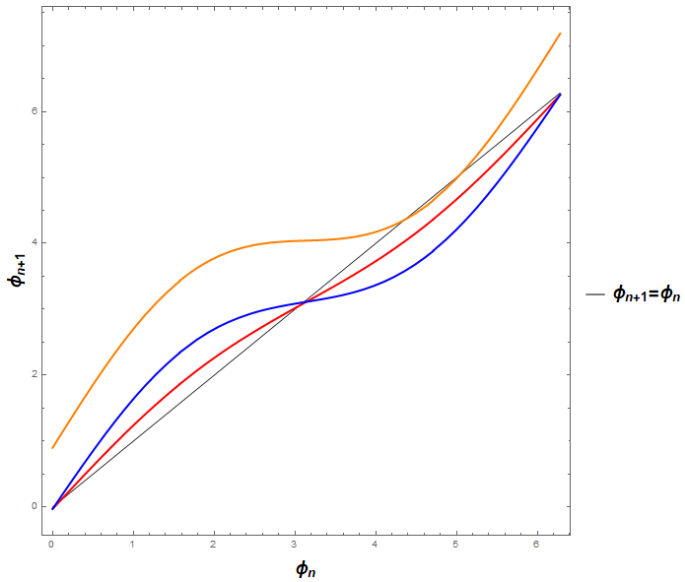

Figure 3.4: Dynamics of the phase difference of clocks $C1$ and $C2$. An increase in the magnitude of the perturbation α increases the amplitude of oscillations in the curve, while a smaller α corresponds to a softer curve (blue and red curves, respectively). An increase in the phase difference, ϵ, shifts the curve (yellow), but for a sufficiently large α, we can still find fixed points.

As in the work [23], it was proved that the phase difference given by $\Omega(\phi_n)$ has one stable fixed point, ϕ_f^s, and one unstable, ϕ_f^u. The value found for the stable fixed point is, in first order approximation, $\phi_f^s = \pi + \arcsin\left(\frac{\pi h^2 \epsilon}{8\alpha\mu}\right)$, whereas the unstable fixed point holds the value of $\phi_f^u = -\arcsin\left(\frac{\pi h^2 \epsilon}{8\alpha\mu}\right)$. When natural angular frequencies are very near, that is, for small values of ϵ, we have that $\phi_f^s \approx \pi$ and $\phi_f^u \approx 0$. Our interest lies essentially on the stable fixed point, whose value indicates that the system of two coupled clocks with similar natural oscillation frequencies tend to stabilize in phase opposition.

An important remark to make is the fact that in the work of [23], the values found for fixed points are $\phi_f^s = \pi - \arcsin\left(\frac{\pi h^2 \delta}{4\alpha\mu}\right)$ and $\phi_f^u = \arcsin\left(\frac{\pi h^2 \delta}{4\alpha\mu}\right)$. However, in that case, the angular velocity was considered to be, for each clock, $\omega_1 = \omega - \delta$ and $\omega_2 = \omega + \delta$. Thus, the difference of natural frequencies between both clocks is given by $\omega_2 - \omega_1 = 2\delta$. Here in this work, we considered $\omega_1 = \omega$ and $\omega_2 = \omega + \epsilon$, so that $\epsilon = 2\delta$, reason why we present here a difference in the argument of the $\arcsin$ function by a factor of 2. Also, the sign is different as well. This is because in [23] $C2$ was the reference clock, that is, the fastest one, while in this work we considered $C1$, the slowest. While for the case $1:1$ we observe a mere change of sign in the component $\arcsin\left(\frac{\pi h^2 \delta}{4\alpha\mu}\right)$ when we switch both clocks, obviously this no longer works for $N:1$ when $N > 1$. In the latter case, the problem holds no longer any symmetry between the clocks when $\epsilon = 0$.

3.2 A 2:1 Frequency Relation

In this section we present new results.

When we increase the velocity of the fastest clock ($C2$) to $2\omega + \epsilon$, considering that $\epsilon << \omega$, we expect $C2$ to complete approximately two laps for each lap of $C1$. Consequently, because $C2$ crosses the vertical position twice as many times as $C1$ does, we expect 2 impulses felt by $C1$ and 1 impulse felt by $C2$. The proceeding is similar to the case $1:1$. We have, for a frequency relation of $2:1$, $\omega_2 = 2\omega_1 + \epsilon$, the following reasoning:

$$\begin{cases} \Phi_1(t_0^-) = 0^- \\ \Phi_2(t_0^-) = \phi_0, \end{cases} \tag{3.13}$$

with $\Phi_2(t_0^-) - \Phi_1(t_0^-) = \phi_0 - 0 = \phi_0$ as the initial phase difference, which is going to be mapped to ϕ_{n+1} along the cycles. When the first kick is given, from $C1$ to $C2$,

$$\begin{cases} \Phi_1(t_0^+) = 0^+ \\ \Phi_2(t_0^+) = \sigma(\phi_0, \omega_2, \alpha). \end{cases} \tag{3.14}$$

The next time instants to consider are

$$\begin{cases} \Phi_1(t_1^-) = \Phi_1(t_0^+) + \omega_1\left(\frac{\Phi_2(t_1^-) - \Phi_2(t_0^+)}{\omega_2}\right) = \frac{\omega_1}{\omega_2}(2\pi - \sigma(\phi_0, \omega_2, \alpha)) \\ \Phi_2(t_0^-) = 2\pi^-. \end{cases} \tag{3.15}$$

The second kick is given from $C2$ to $C1$,

$$\begin{cases} \Phi_1(t_1^+) = \sigma(\frac{\omega_1}{\omega_2}(2\pi - \sigma(\phi_0, \omega_2, \alpha))) \\ \Phi_2(t_1^+) = 2\pi^+. \end{cases} \tag{3.16}$$

The next time instants to consider are

$$\begin{cases} \Phi_1(t_2^-) = \Phi_1(t_1^+) + \omega_1\left(\frac{\Phi_2(t_2^-) - \Phi_2(t_1^+)}{\omega_2}\right) = \sigma(\frac{\omega_1}{\omega_2}(2\pi - \sigma(\phi_0, \omega_2, \alpha))) + 2\pi\frac{\omega_1}{\omega_2} \\ \Phi_2(t_2^-) = 4\pi^-. \end{cases} \tag{3.17}$$

The third kick is given from $C2$ to $C1$ again,

$$\begin{cases} \Phi_1(t_2^+) = \sigma(\sigma(\frac{\omega_1}{\omega_2}(2\pi - \sigma(\phi_0, \omega_2, \alpha)), \omega_1, \alpha) + 2\pi\frac{\omega_1}{\omega_2}, \omega_1, \alpha) \\ \Phi_2(t_2^+) = 4\pi^+. \end{cases} \tag{3.18}$$

At last, the final time instant is t_3^-, which marks the end of the cycle for both clocks:

$$\begin{cases} \Phi_1(t_3^-) = 2\pi^- \\ \Phi_2(t_3^-) = \Phi_2(t_2^+) + \omega_2\left(\frac{\Phi_1(t_3^-)-\Phi_1(t_2^+)}{\omega_1}\right) = \\ = 4\pi + \frac{\omega_2}{\omega_1}\left(2\pi - \sigma(\sigma(\frac{\omega_1}{\omega_2}(2\pi - \sigma(\phi_0, \omega_2, \alpha)), \omega_1, \alpha) + 2\pi\frac{\omega_1}{\omega_2}, \omega_1, \alpha)\right). \end{cases} \tag{3.19}$$

The final phase difference at the end of the first cycle is given by

$$\phi_1 = \Phi_2(t_3^-) - \Phi_1(t_3^-) =$$

$$= 2\pi + \frac{\omega_2}{\omega_1}\left(2\pi - \sigma(\sigma(\frac{\omega_1}{\omega_2}(2\pi - \sigma(\phi_0, \omega_2, \alpha)), \omega_1, \alpha) + 2\pi\frac{\omega_1}{\omega_2}, \omega_1, \alpha)\right) \tag{3.20}$$

$$\Leftrightarrow \phi_1 = \Omega_{2:1}(\phi_0),$$

which, generalizing, becomes

$$\phi_{n+1} = \Omega_{2:1}(\phi_n), \tag{3.21}$$

where $\Omega_{2:1}$ is a function that maps values of phase difference at time t_n^-, ϕ_{n+1} to the final phase difference between the two clocks at time t_{n+1}^-, ϕ_{n+1}.

Figure 3.5 shows the map $\Omega_{2:1}$ in contrast with the map for the 1:1 case, $\Omega_{1:1}$. As we should expect, both maps are 2π-periodic, and this must happen, naturally, for every map of the phase difference, $\Omega_{N:1}$, since their respective domain is defined by the interval $[0, 2\pi[$. In figure 3.5 we can compare dynamics of both frequency relations as a function of phase detuning as we fixed the perturbation parameter at the value $\alpha = 0.5$. This is, of course, an exaggerated value, since the curvature of the map is very subtle for the real experimental values ($\sim 10^{-4}$, according to [23]). We verify, in figure 3.5b, that for the same intensity of perturbation, both maps $\Omega_{1:1}$ and $\Omega_{2:1}$ shift upwards with the detuning, ϵ. For $\epsilon \neq 0$, the fixed points do not coincide any more, which is natural, since in each map composition, the point of intersection $\Omega_{N:1}(\phi) = \phi$ is not affected by the value of the parameter α. This said, any change in the angular velocity ($\omega + \epsilon$) by means of the increase or decrease of ϵ can be noticed with greater emphasis. Both compositions have different analytical structures, and that is why we see a difference in the equilibrium points when changing the detuning parameter.

The values for the fixed points found for the map $\Omega_{2:1}$ are $\phi_f^s = \pi + \arcsin\left(\frac{h^2\pi\epsilon}{2\alpha\mu}\right)$ and $\phi_f^u = -\arcsin\left(\frac{h^2\pi\epsilon}{2\alpha\mu}\right)$, which differs from the values found for the fixed points of the map $\Omega_{1:1}$ by a factor of $\frac{1}{4}$ in the argument of the $\arcsin$ function. We analyze that for a null value of ϵ, the fixed points coincide in first order for maps $\Omega_{1:1}$ and $\Omega_{2:1}$, and we recover the symmetry of the problem. However, the displacement term of the stable fixed point, $\arcsin$, is greater for the map $\Omega_{2:1}$ and thus, for increasing values of ϵ, by looking at figure 3.5, we observe a shift of the intersection $\phi_{n+1} = \phi$ to the right much more rapidly for map $\Omega_{2:1}$ than for $\Omega_{1:1}$.

Again, for $\epsilon << 1$, that is, very near natural frequencies, we observe that $\phi_f^s \approx \pi$ and $\phi_f^u \approx 0$, therefore we expect the clocks to synchronize in phase opposition. In this case, however, when we speak of phase opposition we mean a *generalized phase opposition*. When phase locking occurs in the case of a $1:1$ frequency relation, both clocks oscillate with a continuous phase difference of approximately π between them. In the case of a $2:1$ frequency relation, when phase locking occurs, that does not happen quite exactly in the same way. Because both clocks have different velocities, their phase difference will always be changing along each cycle. The important issue is that, when we analyze the phase difference at a specific point of the cycle (may be the starting or ending point), they preserve a phase difference of approximately π, regardless of the phase evolution inside each cycle. To that conservation of the phase difference (in this case the value is π) we call *generalized phase opposition*.

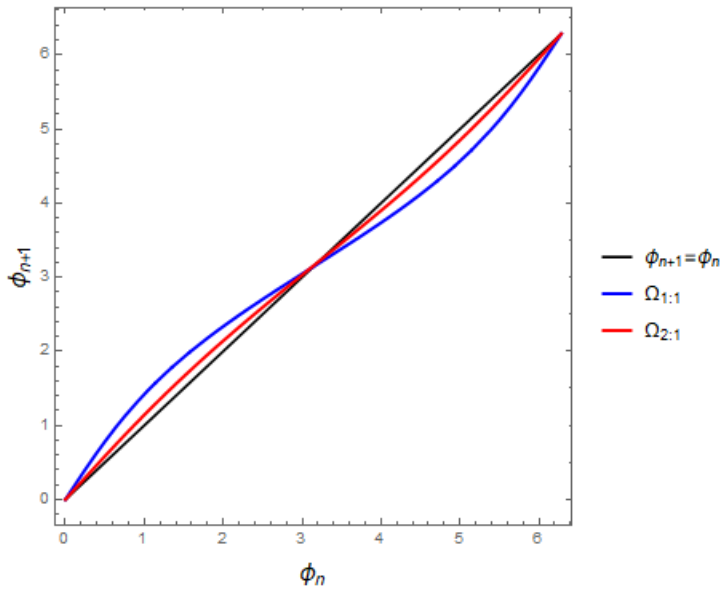

(a) $\alpha = 0.5$, $\epsilon = 0$

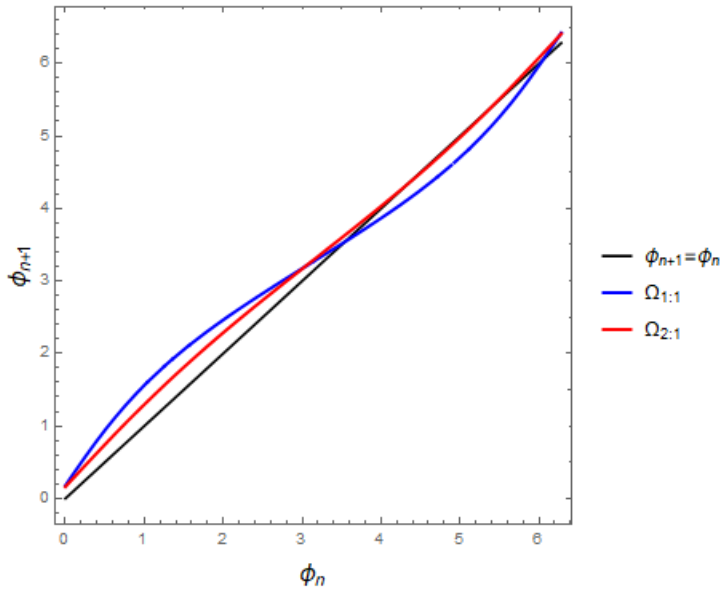

(b) $\alpha = 0.5$, $\epsilon = 0.1$

Figure 3.5: Dynamics of the maps $\Omega_{1:1}$ and $\Omega_{2:1}$ for different values of ϵ, represented by the blue and red curves, respectively.

4 Stability and Numerical Simulations

4.1 Linear Expansions

The discussion of this paragraph is based in the theory of [27], but the results are new. We review some classic results and general theory based on continuous models. The phase evolution of a self-sustained oscillator with natural frequency ω_0 is given by

$$\begin{aligned} \frac{d\Phi(t)}{dt} &= \omega_0 \\ \Leftrightarrow \Phi(t) &= \Phi(0) + \omega_0\, t. \end{aligned} \tag{4.1}$$

We have seen in sections 2 and 3 that we have an attractive fixed point for $v_{n+1} = P(v_n)$. Physically, this means that the velocity of the oscillator (the amplitude of the limit cycle) tends towards a certain value after n oscillations. When the system is facing a weak interaction, which is the case, we can make

a description by "phase approximation", where we neglect variations in the amplitude of the limit cycle (that we will treat in section 5) and consider only the dynamics of the phase. Thus, for small forcing η_0, the equations of motion of a general periodically forced dynamical system in the vicinity of a limit cycle can be reduced to

$$\frac{d\Phi}{dt} = \omega_0 + \eta_0\, Q(\Phi, t). \tag{4.2}$$

The function $Q(\Phi, t)$ is 2π-periodic in the phase and T-periodic in time, where T is the period of oscillations. Thus, the phase space of the dynamical system 4.2 is a two-dimensional torus surface with domain $0 \leq \Phi < 2\pi$, $0 \leq t < T$ (this geometric issue will also be treated in section 5).

For two coupled oscillators (1 and 2) with the same type of dynamics of that of equation 4.2, the dynamics of the new system can be written, taking as reference the oscillator 1, as

$$\frac{d\Phi_2}{dt} - \frac{d\Phi_1}{dt} = \omega_2 - \omega_1 + \eta_2\, Q_2(\Phi_2, t) - \eta_1\, Q_1(\Phi_1, t), \tag{4.3}$$

where ω_1 and ω_2 are, respectively, the natural frequencies of oscillators 1 and 2. Integrating the previous expression and considering an equal reciprocal interaction, $\eta_1 = \eta_2 = \eta$ and that the term $Q_2(\Phi_2, t) - Q_1(\Phi_1, t) = \eta\, F(\Phi_2(t) - \Phi_1(t), t))$, we have

$$\Phi_2(t) - \Phi_1(t) = \Phi_2(0) - \Phi_1(0) + (\omega_2 - \omega_1)t + \eta\, F(\Phi_2(t) - \Phi_1(t), t), \tag{4.4}$$

which is the celebrated Adler equation [2], that expresses the evolution of the phase difference between two coupled oscillators, that is,

$$\phi(t) = \phi(0) + (\omega_2 - \omega_1)t + \eta\, F(\phi(t), t), \tag{4.5}$$

where $\phi(t) = \Phi_2(t) - \Phi_1(t)$.

If we fix the value of ϕ and consider its evolution at every n-th cycle (a stroboscopic mapping with a periodicity T, that is, $\phi(t) \to \phi(t + T)$), by choosing a multiple of the period, $t = nT$, we have a correspondence between the points of phase $\Phi(t)$ and $\Phi(t + nT)$, given by the map:

$$\phi((n + 1)T) = \phi(nT) + (\omega_2 - \omega_1)nT + \eta\, F(\phi(nT), n). \tag{4.6}$$

If $F(\phi(nT), n)$ does not depend explicitly on n, that is, $F(\phi(nT), n) = \tilde{F}(\phi_n)$, which is the autonomous case, we have

$$\phi_{n+1} = \phi_n + (\omega_2 - \omega_1)nT + \eta\, \tilde{F}(\phi_n), \tag{4.7}$$

which is the discrete Adler equation 4.7 for the evolution of the phase difference between both oscillators. Note that the separation between the drifting term (the difference of frequencies, $(\omega_2 - \omega_1)nT$) and the nonlinear coupling function $\tilde{F}(\phi_n)$ is valid only for small η, otherwise both terms depend on both the amplitude and difference of frequencies.

We apply the discrete Adler equation to the dynamics of our two coupled Andronov clocks. The coupling function consists of the sum of the periodic impulses felt by each clock. We count, for each cycle, 1 impulse received by the escapement of $C1$ and N impulses received by the escapement of $C2$. Thus, $C2$ is perturbed once and $C1$ is perturbed N times. Furthermore, the coupling function is T-periodic, so it does not depend on the cycle, *i.e.*, $F(\phi(nT), n) = \tilde{F}(\phi_n)$, as expressed in equation 4.7. Our model of coupling, referenced to $C1$, is therefore

$$\begin{aligned} \eta\, \tilde{F}(\phi_n) &= \sum_{i=1}^{M} \text{impulses from } C2 - \sum_{i=1}^{N} \text{impulses from } C1 \\ \Leftrightarrow \eta \tilde{F}(\phi_n) &= \sum_{i=1}^{N} \sigma(\phi_i, \omega_1, \alpha) - \sigma(\phi_n, \omega_2, \alpha) \end{aligned} \tag{4.8}$$

We take the expression of the perturbation 3.3 and perform a linear approximation around $\alpha = 0$. We get

$$\sigma(\phi_n, \omega, \alpha) = \frac{\pi}{2} - \phi_n - \frac{\alpha\ sin(\phi_n)}{\gamma(\phi, \omega)}, \tag{4.9}$$

which means that under a small perturbation α, the effect of a clock over the other is, in first order, to subtract the amount $\frac{\alpha\ sin(\phi_n)}{\gamma(\phi,\omega)}$ to the phase $\phi - \frac{\pi}{2}$ (the beginning of an oscillation is at the top of the limit cycle, *i.e.*, $\frac{\pi}{2}$ radians before). In the case of $C2$, this subtraction is performed N times. For the sake of simplicity, we consider that the effect perturbation has always the same value, that is, $\alpha_i = \alpha$. We get

$$\begin{aligned} \eta\tilde{F}(\phi_n) &= \left(\frac{\pi}{2} - \phi_n - \alpha\sum_{i=1}^{N}\frac{\sin\phi_i}{\gamma(\phi_i,\omega_1)}\right) - \left(\frac{\pi}{2} - \phi_n - \alpha\frac{\sin\phi_n}{\gamma(\phi_n,\omega_2)}\right) \\ \Leftrightarrow \eta\tilde{F}(\phi_n) &= -\alpha\sum_{i=1}^{N}\frac{\sin\phi_i}{\gamma(\phi_i,\omega_1)} + \alpha\frac{\sin\phi_n}{\gamma(\phi_n,\omega_2)}. \end{aligned} \tag{4.10}$$

Therefore, when we normalize equation 4.7 to the first turn of the limit cycle of $C1$, we get

$$\begin{aligned} \phi_{n+1} &= \phi_n + (\omega_2 - \omega_1)T + \eta\,\tilde{F}(\phi_n) \\ \Leftrightarrow \phi_{n+1} &= \phi_n + \frac{\omega_2 - \omega_1}{\omega_1}2n\pi + \alpha\frac{\sin\phi_n}{\gamma(\phi_n,\omega_2)} - \alpha\sum_{i=1}^{N}\frac{\sin\phi_i}{\gamma(\phi_i,\omega_1)} \\ \Leftrightarrow \phi_{n+1} &= \phi_n + (N-1)2\pi + \frac{\epsilon}{\omega}2\pi + \alpha\frac{\sin\phi_n}{\gamma(\phi_n, N\omega+\epsilon)} - \alpha\sum_{i=1}^{N}\frac{\sin\phi_i}{\gamma(\phi_i,\omega)}, \end{aligned} \tag{4.11}$$

where $\eta = \frac{\alpha}{\gamma(\phi,\omega(\epsilon))}$. This expansion is only possible due to small intensities of perturbation (as we will see later, a *small* α corresponds to $\alpha < h$) – in the work of [23], experiments for a $1:1$ frequency relation reveal values of perturbation of the order of 10^{-4}.

A map of the expansion that defines the dynamics of the phase difference of the system of coupled clocks is, therefore, defined as

$$\phi_{n+1} = \Xi_{N:1}(\phi), \tag{4.12}$$

where

$$\Xi_{N:1}(\phi) = \phi + (N-1)2\pi + \frac{\epsilon}{\omega}2\pi + \alpha\frac{\sin\phi}{\gamma(\phi, N\omega+\epsilon)} - \alpha\sum_{i=1}^{N}\frac{\sin(r(\phi,N))}{\gamma(r(\phi,N),\omega)}, \tag{4.13}$$

and where

$$r(\phi, N) = \frac{2k\pi - \phi}{N\omega + \epsilon}\,\omega \tag{4.14}$$

is just another form of mapping the phase of a clock after it performs a sweeping action along the limit cycle.

Note that for a frequency relation of $1:1$ the problem is only symmetric if both velocities ω_1 and ω_2 are the same. In that case, the clocks are indistinguishable and the system is invariant under their exchange. However, in this case, we have a shift in the velocities, ϵ, which confers different characteristics to each clock. Now we can distinguish both clocks. As $N = 1$, the equation 4.13 becomes simply

$$\begin{aligned} \Xi_{1:1}(\phi) &= \phi + 2\pi\,\frac{\epsilon}{\omega} + \frac{\alpha\ \sin(\phi)}{\gamma(\phi,\ \omega+\epsilon)} - \frac{\alpha\ \sin(r(\phi,1))}{\gamma(r(\phi,1),\omega)} \\ \Leftrightarrow \Xi_{1:1}(\phi) &= \phi + 2\pi\,\frac{\epsilon}{\omega} + \frac{\alpha\ \sin(\phi)}{\gamma(\phi,\ \omega+\epsilon)} - \frac{\alpha\ \sin(\frac{2\pi-\phi}{\omega+\epsilon}\,\omega)}{\gamma(\frac{2\pi-\phi}{\omega+\epsilon}\,\omega,\omega)}, \end{aligned} \tag{4.15}$$

While the third term on the right hand side of equation 4.15 corresponds to the influence of the perturbation α on the clock $C2$, the fourth term has the same purpose, but related to clock $C1$. In fact, equation 4.13 can be written, in first order, as

$$\Xi_{1:1}(\phi) = \phi + 2\pi\,\frac{\epsilon}{\omega} + \frac{\alpha\ \sin(\phi_2)}{\gamma(\phi_2,\ \omega_2)} - \frac{\alpha\ \sin(\phi_1)}{\gamma(\phi_1\ ,\omega_1)} + O(\epsilon^2). \tag{4.16}$$

As we observe, we have positive and negative terms that are directly related to the interactions shared in the system. Intuitively, under the change of two clocks ($C1 \leftrightarrow C2$), we verify this antisymmetric property. This $1:1$ symmetry-type feature endows the system with a *master-master* relation. This happens only for this case once that, for $N > 1$, one of the interaction terms of 4.13 loses relevance over the other, that is, $\alpha \sum_{k=1}^{N} \approx 0$. These observations motivate us to conjecture the following:

Conjecture:
The relation between two Andronov clocks for $N:1$, where $N > 1$, with an interaction of the same type, that is, $\pm\alpha$, is always master-slave.

Another feature on which we can look into is the periodicity. When $\epsilon = 0$ and $\frac{\omega_2}{\omega_1} = N \in \mathbb{N}$, we have $r(\phi, N) = \frac{2k\pi - \phi}{N}$ and, because $\sin(\phi)$ and $\gamma(\phi, \omega)$ are 2π-periodic functions, equation 4.13 becomes

$$\Xi_{N:1}(\phi) = \phi + \frac{\alpha\ \sin(\phi)}{\gamma(\phi, N\omega)} + \sum_{k=1}^{n} \frac{\alpha\ \sin(\frac{\phi}{N})}{\gamma(-\phi, \omega)}. \tag{4.17}$$

The dominant term, $\frac{\alpha\ \sin(\phi)}{\gamma(\phi, nw)}$, which represents the kick from the slowest to the fastest clock, dictates the 2π-periodic character of the linear map. We see in figure 4.1 that, for an $\epsilon = 0$, there is no shift and the fixed points remain at the same angular coordinate, $\phi^* \approx \pi$. A value $\epsilon \neq 0$ affects the phase argument in the function γ, which induces a shift on every points of stability.

4.2 Second Order Expansions

In subsection 4.1 we looked at the linear expansions and found how they might be useful, in the sense that it becomes very easy to manipulate them – for instance, to find regions of synchronization, by calculating the Arnold tongues, which is a new result, see subsection 4.3. We now take a look at the second order expansion of the map $1:1$. We are interested in analyzing the behavior of the dynamics through the form of the map expanded around $\alpha = 0$ and $\epsilon = 0$. We present calculations just for the case $1:1$, although we have very good results – in the sense they are valid and physically meaningful – for the case $2:1$ as well. Further development of this study will be addressed in future work, since the formulae are very long and beyond the scope of a master thesis.

We first consider the map responsible for the effect of the impulses on the phase of the representative point on the limit cycle (expression 3.3),

$$\sigma(\phi_i, \omega_i, \alpha_i) = \arctan\left(\sin(\phi_i), \cos(\phi_i) - \frac{\alpha_i}{\gamma(\phi_i, \omega_i)}\right), \quad i = 1, 2. \tag{4.18}$$

We only consider the middle branch of the function $\gamma(\phi_i, \omega_i)$, that is, in the domain $\frac{\pi}{2} \leq \phi < \frac{3\pi}{2}$, because we are interested in the form of the map near the attractive fixed point, which is the asymptotic stable equilibrium point. Thus, we consider

$$\gamma(\phi_i, \omega_i) = \frac{h^2\omega_i}{8\mu}, \qquad \frac{\pi}{2} \leq \phi_i < \frac{3\pi}{2}. \tag{4.19}$$

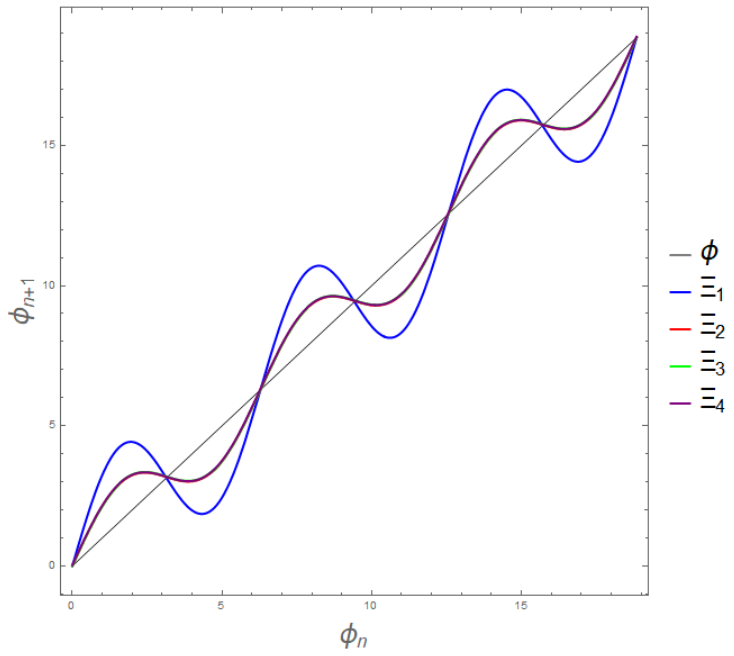

(a) $\epsilon = 0.8$

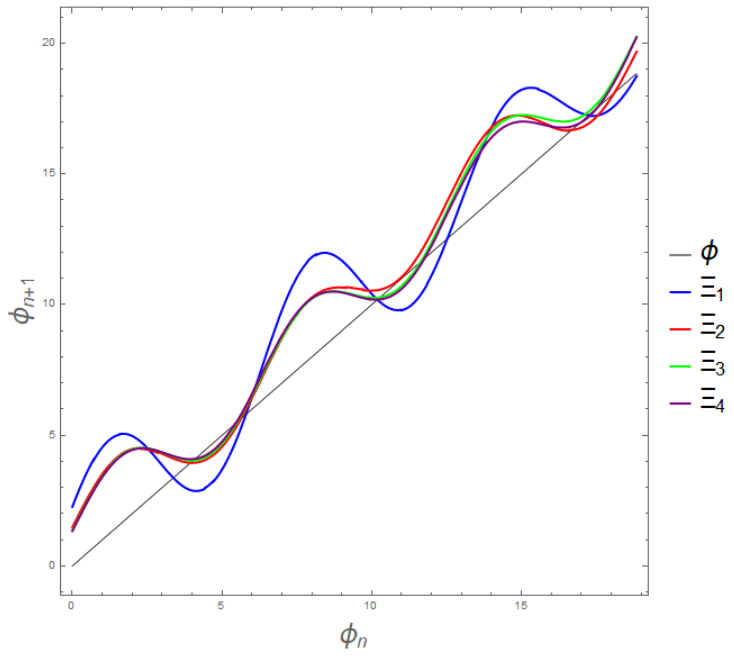

(b) $\epsilon = 0$

Figure 4.1: Linear expansions of the maps Ξ_1 (blue), Ξ_2 (red), Ξ_3 (green) and Ξ_4 (purple). The respective fixed points coincide when $\epsilon = 0$. In figure b) we observe an upward shift of the curve and, consequently, a shift in the equilibrium points, generated by a positive value of ϵ.

This does not constitute any problem, since we are too far from the critical points of discontinuity in the limit cycle. Anyway, even if we had to treat such discontinuities, we are dealing with very low values of dry friction, μ, meaning that the radius almost coincides in those points.

The expansion is performed around $\alpha = 0$ until order 2. It is irrelevant to expand around $\epsilon = 0$, since the only dependence on ϵ lies in the function γ, when σ is referring to the fastest clock, with velocity $\omega + \epsilon$ – and the expansion of $\frac{h^2(\omega+\epsilon)}{8\mu}$ in ϵ is trivial, leaving the formulae unchanged.

We use it in the argument of the map 4.18 to expand it. We get

$$\sigma_{exp}(\phi_i, \omega_i, \alpha_i) = \phi + \frac{8\,\mu \sin(\phi)}{h^2\omega}\,\alpha + \frac{32\,\mu^2 \sin(2\phi)\alpha^2}{h^4\omega^2}\,\alpha^2. \tag{4.20}$$

Expanding until the second order is useful in the sense that the level of smallness given by the parameter α provides a much more realistic approximation to the original map, still allowing equations being easy to work with.

We now introduce the map expressed in 4.20 in the 4-map composition of the system of two coupled clocks. Analogously to the expression 3.11 and represented by 3.12, we get

$$\Omega_{1:1}(\phi_{n+1}) = r(\sigma_{exp}(r(\sigma_{exp}(\phi_n, \omega_2, \alpha), d_1), \omega_1, \alpha), d_2), \tag{4.21}$$

where $d_1 = d_2^{-1} = \frac{\omega_1}{\omega_2}$. We then perform a linear expansion until the second order around $\alpha = 0$ and $\epsilon = 0$, so that we get

$$\begin{aligned}\Xi^{(2)}_{1:1}(\phi) = \phi + 2\pi\,\frac{\epsilon}{\omega} + \frac{8\mu}{h^2\omega}\,2\sin(\phi)\,\alpha\; + \;\frac{8\mu}{h^2\omega}\cos(\phi)(2\pi - \phi)\,\frac{\epsilon}{\omega}\,\alpha + \\ + \left(\frac{8\mu}{h^2\omega}\right)^2 3\cos(\phi)\sin(\phi)\,\alpha^2,\end{aligned} \tag{4.22}$$

where the superscript (2) is, of course, the notation for the second order expansion. The common factor $\frac{8\mu}{h^2\omega}$ comes from the fact that we are dividing by the function γ in the domain $\frac{\pi}{2} \leq \phi < \frac{3\pi}{2}$.

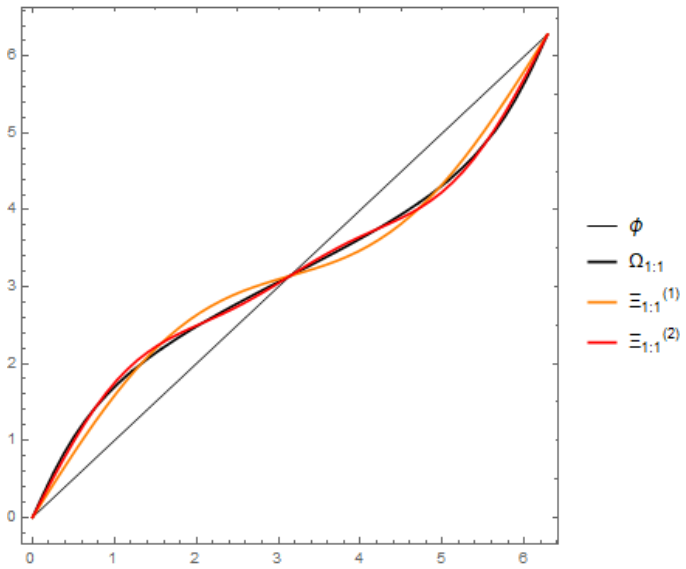

Figure 4.2: Comparing the original map (black) with it 1st order (orange) and 2nd order (red) expansions for the case $1:1$. We observe that the 2nd order expansion is much more in agreement with the original map than the 1st order expansion. The values chosen for the relevant parameters are:$\alpha = 0.8$, $\epsilon = 0$ and $\mu = 0.00025$. The value of the perturbation α does not correspond to the order of magnitude of the experimental values, but it is emphasized here to show the discrepancy between expansions.

4.3 Arnold Tongues

The Arnold tongue, named after Vladimir Arnold, is a region in parameter space where the system is in a synchronous regime [27]. In this context, it is our interest to find out the limits of stability of the system in the (ϵ, α) parameter space. Intuitively, the idea is based on a graphical analysis of the maps. As explained in figure 3.4, every change in ϵ corresponds to a shift of the dynamics upwards or downwards, while a change in α changes the intensity of the curve. Graphically this was observed for the map $\Omega_{1:1}$. However, due to the increasing nonlinearity of maps with N, changes in the parameters α and ϵ lead to a much more complex effect. For instance, for maps $\Omega_{2:1}$ and $\Omega_{3:1}$, any change in α affects ϵ and *vice*

versa. We can observe this effect in figure 4.3, which shows how changes in ϵ affect the form of the curves.

We try to find the two fixed points for each map. Then, by fixing a certain value of ϵ, and gradually reduce the value of α, at a certain point the two intersections join together to become one equilibrium point, tangent to $\phi_{n+1} = \phi_n$ (that is, the point where $\phi_f^s = \phi_f^u$), and immediately after, the system finds no more intersections and, therefore, no stability. We then follow the same procedure by iterating ϵ. This is the base for our algorithm.

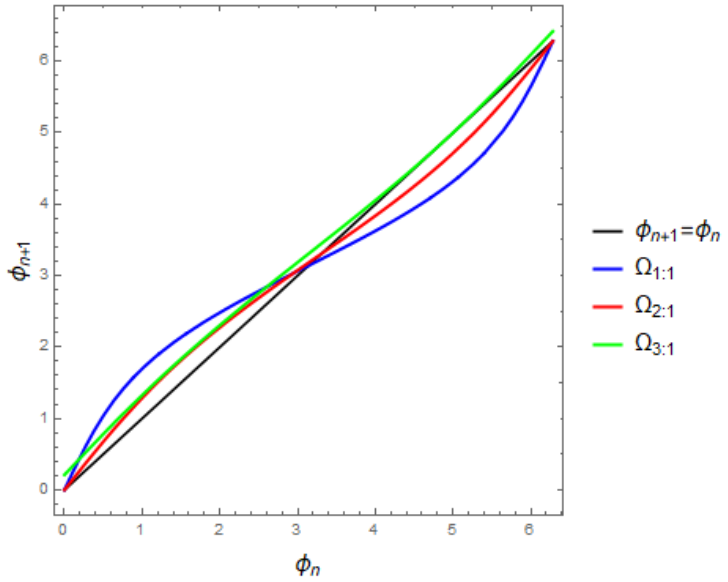

(a) $\epsilon = 0$

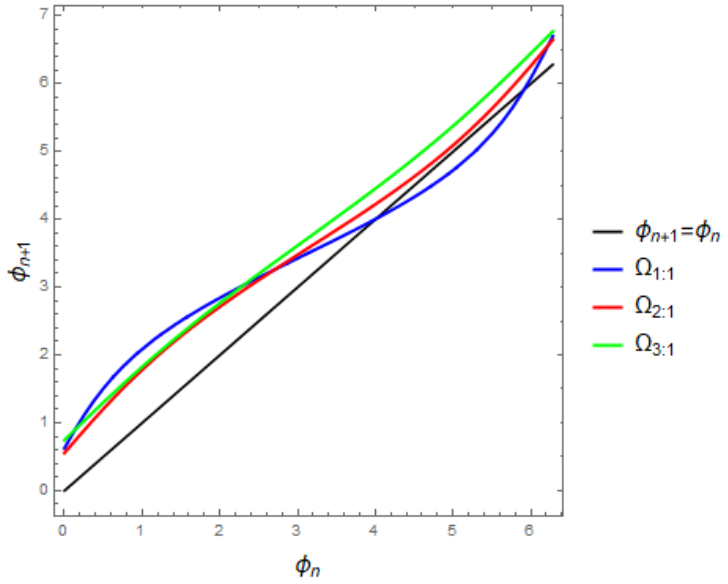

(b) $\epsilon = 0.3$

Figure 4.3: Maps $\Omega_{1:1}$ (blue), $\Omega_{2:1}$ (red) and $\Omega_{3:1}$ (green). When $\epsilon = 0$, we find points of stability only for maps $\Omega_{1:1}$ and $\Omega_{2:1}$. We do find points of stability for map $\Omega_{3:1}$, but for a negative value of ϵ.

By doing this, we are finding several points (ϵ, α) in parameter space that mark the threshold between stable and unstable conditions of the system. This set of points under the conditions above mentioned establishes the threshold between the stable and non-stable regions of the parameter space – the Arnold tongues. By stable and unstable regions we mean the set of parameters α and ϵ that define the conditions which allow the system to synchronize or not, respectively.

So, in the context of our problem, the Arnold tongues are regions of the parameter space, (ϵ, α), for

which we find the system to be stable, meaning that every point of that region corresponds to a set of values for (ϵ, α) for which we can find fixed points for the system. Consequently, knowing that along the n cycles the system tends to the correspondent stable equilibrium phase difference, the two clocks synchronize for that choice of parameters. In figure 4.4 are represented Arnold tongues for the first three orders of synchronization (N-th order is equivalent to $N:1$).

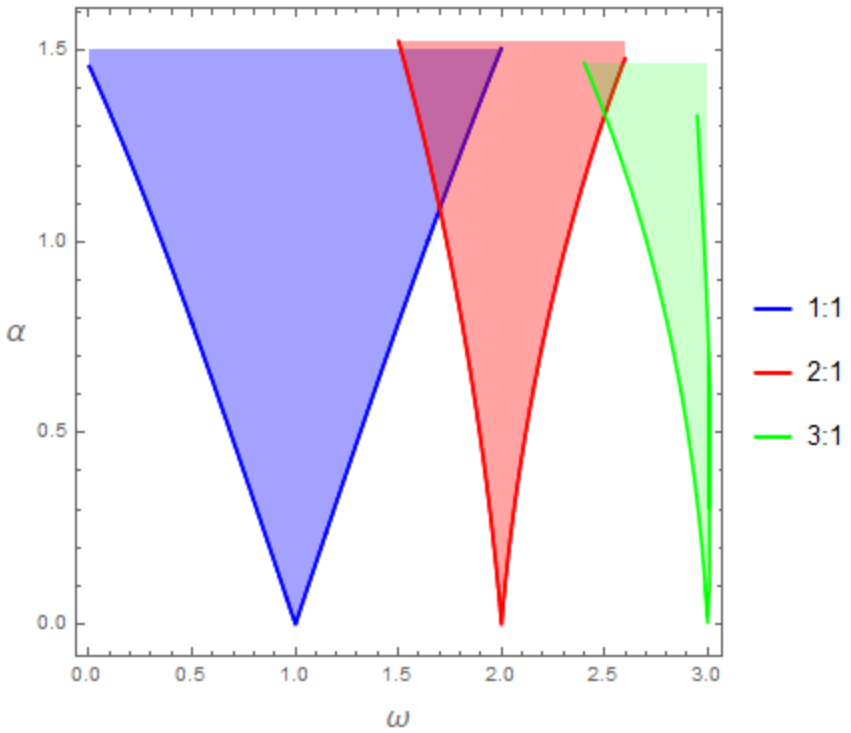

Figure 4.4: Arnold tongues for $1:1$ (blue), $2:1$ (red) and $3:1$ (green) orders of synchronization. The shaded area of the plot delimited by the each solid line corresponds to every pair (ϵ, α) that ensures favorable conditions to the occurrence of synchronization.

Not all the region of the Arnold tongues shown in figure 4.4 corresponds to a valid physical context. In reality, when one clock receives an impulse of kinetic energy from the escapement, $\frac{h^2}{2}$, the effect of its propagation is associated to a certain amount of energy dissipation through the material that connects both clocks. For this reason, the energy felt by the perturbed clock is of much lower intensity than the initial kinetic energy transmitted to the first clock, ΔK. More precisely, the condition that establishes a valid physical context is

$$\alpha^2 < h^2 \Leftrightarrow \alpha < h, \tag{4.23}$$

which corresponds to the definition of a *small* α, in this context. Thus, the shaded area of the plot of figure 4.4 is now delimited also by a superior limit, by the value of $\alpha = h$. This limitation implies a substantial magnification of the image 4.4 and that is why the same synchronization regions for $N = 1, 2, 3$ near $\alpha = 0$ are thinner in figure 4.5.

As we should expect, the Arnold tongues become thinner from $1:1$ to $3:1$, which is natural: the nonlinearity increases with the number of maps in each composition. If we look at the function $\gamma(\phi, \omega)$, the function which provides us the nonlinearity in this system,

$$\gamma(\phi, \omega(\epsilon)) = \begin{cases} \frac{h^2\omega(\epsilon)}{8\mu} + \frac{2\mu}{\omega(\epsilon)}, & 0 \leq \phi < \frac{\pi}{2}, \\ \frac{h^2\omega(\epsilon)}{8\mu}, & \frac{\pi}{2} \leq \phi < \frac{3\pi}{2}, \\ \frac{h^2\omega(\epsilon)}{8\mu} - \frac{2\mu}{\omega(\epsilon)}, & \frac{3\pi}{2} \leq \phi < 2\pi, \end{cases} \tag{4.24}$$

we see that it depends strongly on ϵ, when it is referring to the velocity of the fastest clock, $\omega_2(\epsilon) =$

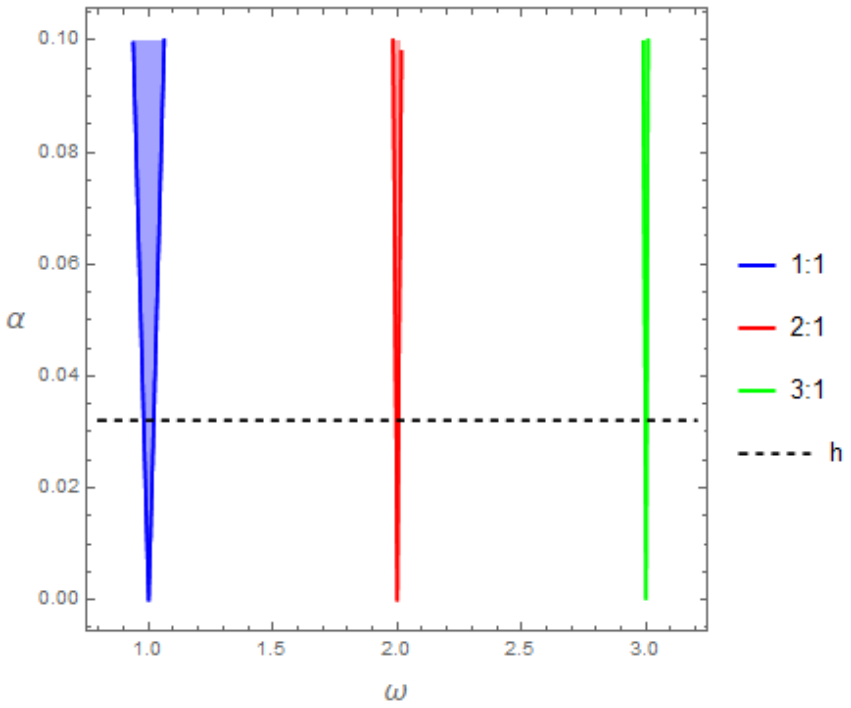

Figure 4.5: Arnold tongues for frequency relations $1:1$ (blue), $2:1$ (red) and $3:1$ (green).The shaded region of the plot is now also delimited by the dashed line, representing the limit value of α for which the system lies under the conditions of a valid physical context.

$N\omega + \epsilon$. The common factor $\frac{h^2\omega(\epsilon)}{8\mu}$ contrasts with the factor $\frac{2\mu}{\omega(\epsilon)}$ in different segments of the limit cycle of the dynamical system and in different quantities. The higher the value of the detuning ϵ, the higher this discrepancy. Consequently, the higher the perturbation α must be to overcome this nonlinear effect. Thus, the higher N, the higher must be the increase of α with ϵ, so that an intersection occurs with $\Omega(\phi_n) = \phi_n$, achieving, that way, synchronization.

The construction of maps $N:1$ is strongly nonlinear due to the discontinuities imposed by γ function (3.4). Naturally we observe that, for significant values of α and ϵ, functions differ accordingly from their respective expansions. We compare the maps with their respective linear expansions in figure 4.6 for frequency relations $1:1$, $2:1$ and $3:1$. Naturally, when we increase the value of the perturbation α, the disparity between the original maps and the linear expansions increases.

These expansions can be used to construct Arnold tongues to study the stability domain when we are facing a very small perturbation and phase detuning. We should expect a match between them and the maps near $(\epsilon, \alpha) = (0, 0)$. Indeed, we see in figures 4.7, 4.8 and 4.9 that the domains of stability for the maps and their expansions are overlapped, especially for values of $\alpha < h$. Also, if we look at the case $1:1$ (figure 4.7), not only do we have a really good match for values of perturbation lower than h, as that match keeps going for values grater than h. However, looking for each of the cases $2:1$ (figure 4.8) and $3:1$ (figure 4.9), we observe a match only for $\alpha < h$ and in the negative slope. This difference is natural, because the first order of the Taylor approximation $\Xi_{N:1}$ is symmetric, whereas the nonlinear maps $\Omega_{N:1}$ are not. Only the second order correction could attenuate this effect (or, just like we did, work the original maps without any changes whatsoever). The linear approximation has the advantage of being much easier to work with, whereas the second order expansion, despite giving us a very good approximation, as we have seen in subsection 4.2, does not bring us any numerical benefits over the original functions, without any approximations. This asymmetry is greater for $N = 3$ than for $N = 2$, which is natural, since the number of compositions and, therefore, the nonlinearity, increases, in respect to one of the clocks (in this case, the slowest clock).

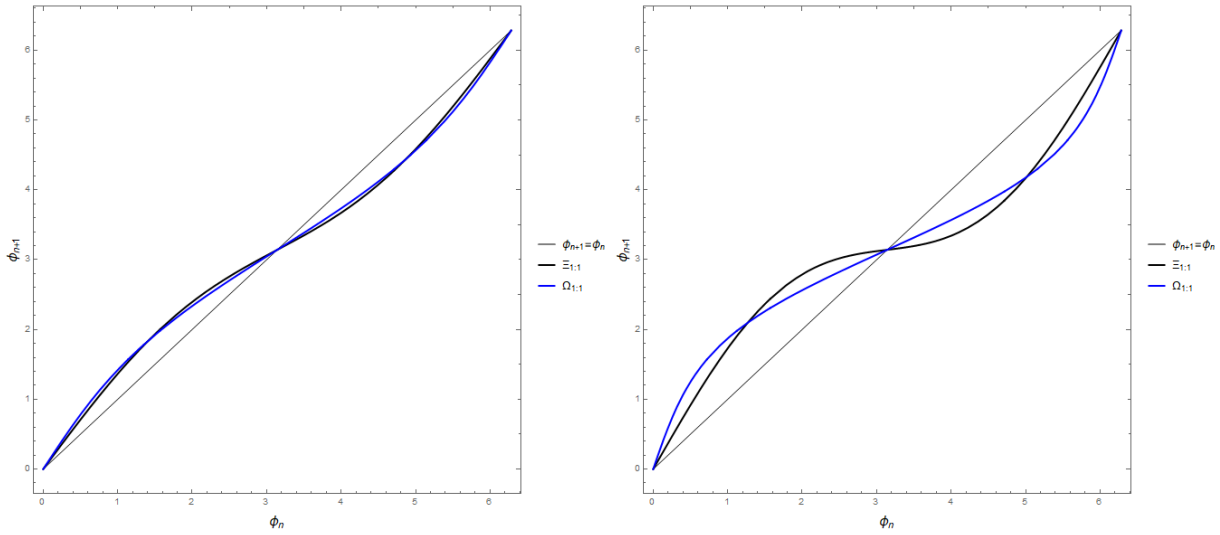

(a) $\Omega_{1:1}$ (blue) and $\Xi_{1:1}$ (black); $\epsilon = 0$, $\alpha = 0.5$.

(b) $\Omega_{1:1}$ (blue) and $\Xi_{1:1}$ (black); $\epsilon = 0$, $\alpha = 1$.

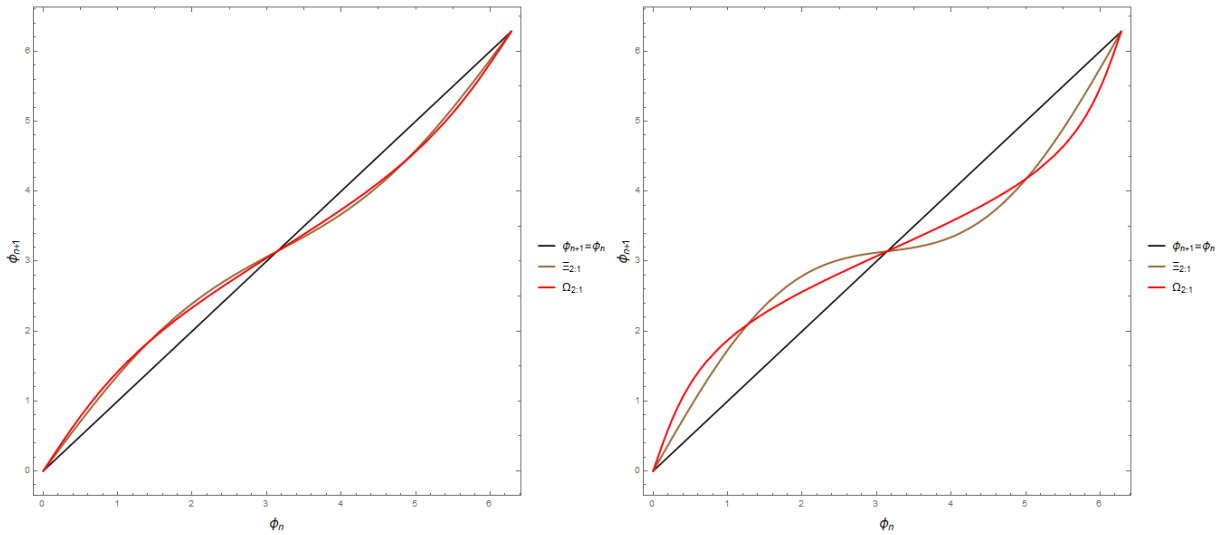

(c) $\Omega_{2:1}$ (red) and $\Xi_{2:1}$ (brown); $\epsilon = 0$, $\alpha = 0.5$.

(d) $\Omega_{2:1}$ (red) and $\Xi_{2:1}$ (brown); $\epsilon = 0$, $\alpha = 1$.

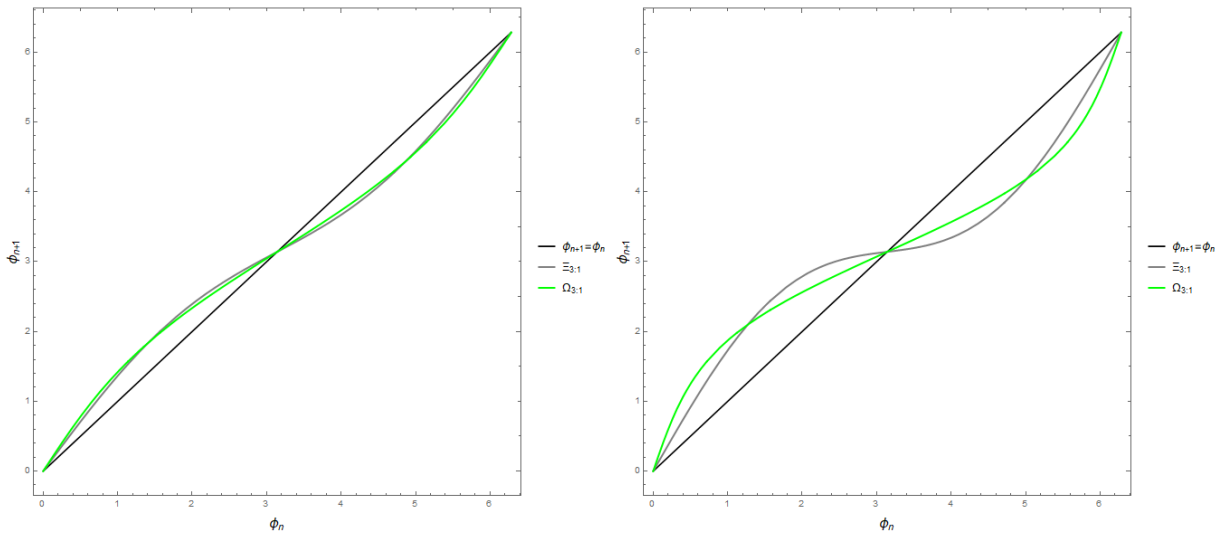

(e) $\Omega_{3:1}$ (green) and $\Xi_{3:1}$ (gray); $\epsilon = 0$, $\alpha = 0.5$.

(f) $\Omega_{3:1}$ (green) and $\Xi_{3:1}$ (gray); $\epsilon = 0$, $\alpha = 1$.

Figure 4.6: Comparing maps of the phase difference with their linear expansions. Figures on the right represent a value of $\alpha = 0.5$ and the ones on the left represent $\alpha = 1$. The match for lower values of α is, as expected, much stronger.

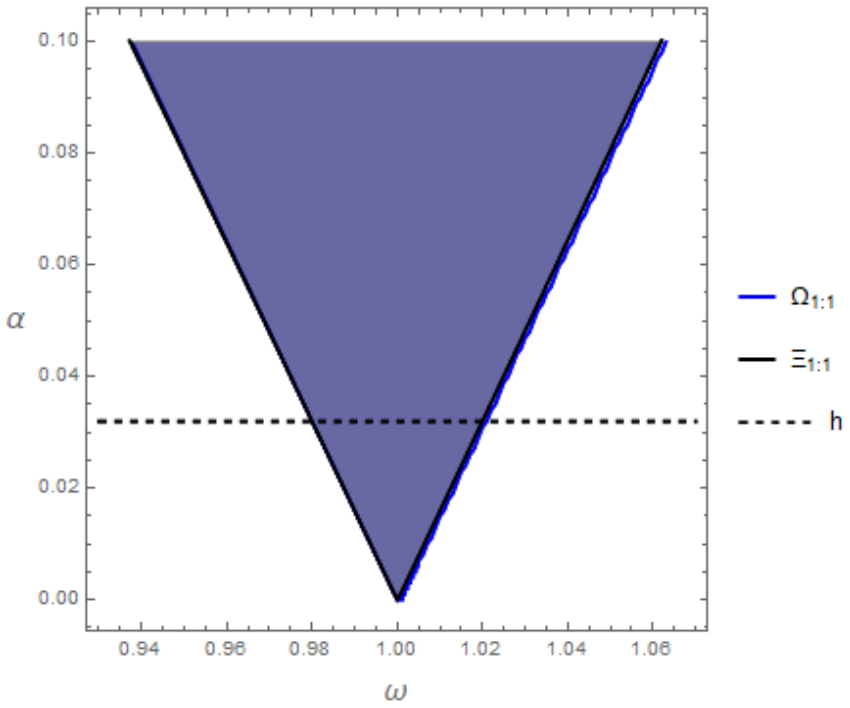

Figure 4.7: Comparison between Arnold tongue of map $\Omega_{1:1}$ (blue) with $\Xi_{1:1}$ (black). We find a very reasonable match, such that both tongues are practically overlapped, being difficult to distinguish them.

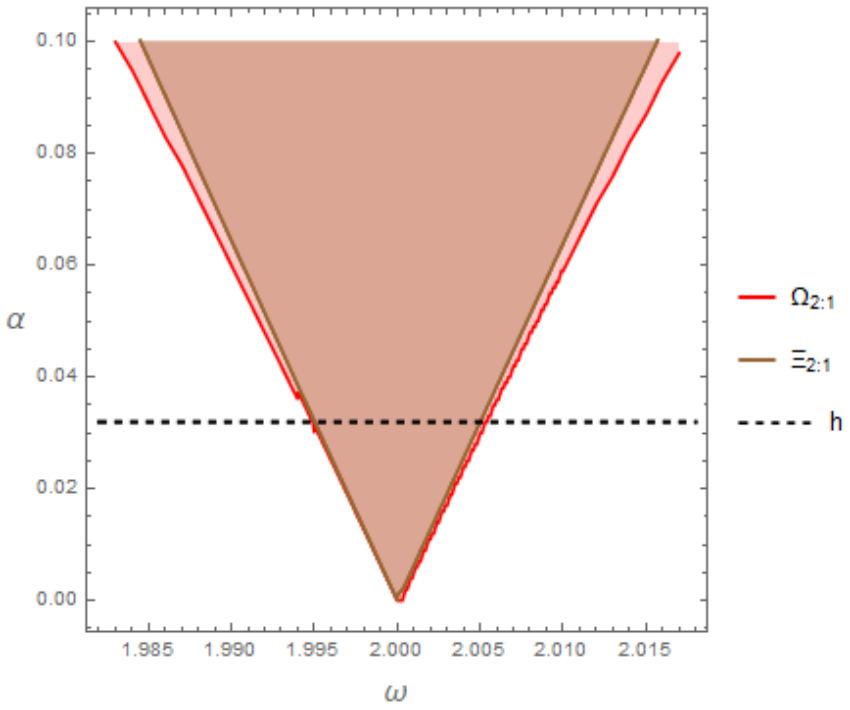

Figure 4.8: Comparison between Arnold tongue of map $\Omega_{2:1}$ (red) with $\Xi_{2:1}$ (brown). We observe a match for $\alpha < h$ and much more for the negative slope of the tongue, corresponding to $\omega_2 = 2\,\omega - \delta$.

When it comes to the effect of friction, by analysis of equation 2.16 if we increase the action of the dry friction from the escapement, the oscillatory system takes less time to achieve the overdamped regime. Another way of seeing this is that the radius decreases faster along the limit cycle. Consequently, in order to maintain the stability of the oscillations (which means to guarantee the closeness of the limit cycle at its initial conditions), a higher value of h must be taken. Thus, more kinetic energy may compensate the energy loss in the contact between the gears. A higher value of h implies necessarily a higher value of α, once that the energy loss along the material that connects both clocks, is the same. But how do we

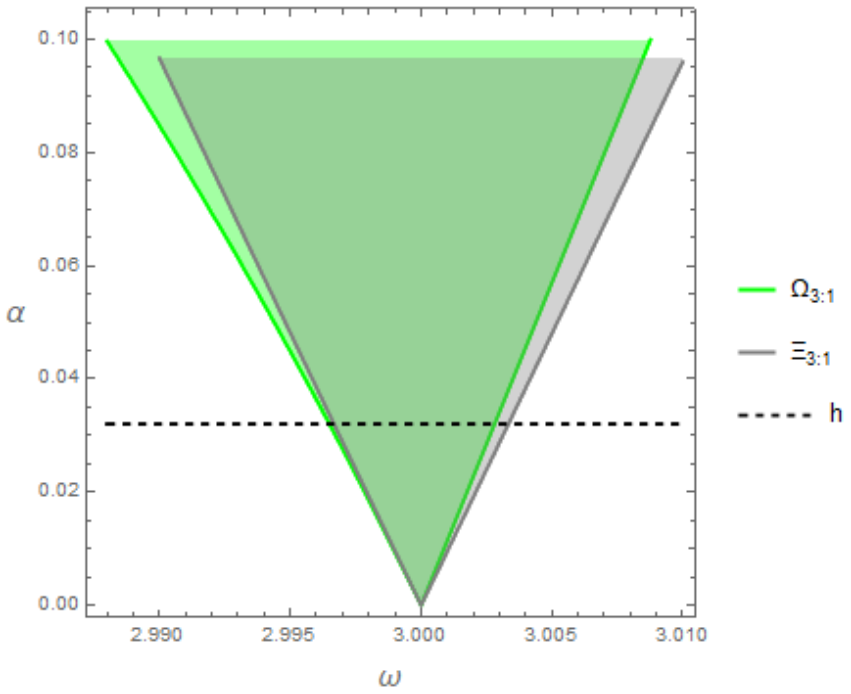

Figure 4.9: Comparison between Arnold tongue of map $\Omega_{3:1}$ (green) with $\Xi_{3:1}$ (gray). We observe a match for $\alpha < h$ and only for the negative slope of the tongue, corresponding to $\omega_3 = 3\,\omega - \delta$.

relate the relation between μ and α with its effect in the Arnold tongues? We answer that question in the following lines.

As mentioned in subsection 3.1, the stable and unstable equilibrium points of the map $\Omega_{1:1}$ computed in the work of [23] are $\phi_f^s = \pi - \arctan(\frac{\pi h^2 \epsilon}{4\alpha\mu})$ and $\phi_f^u = \arctan(\frac{\pi h^2 \epsilon}{4\alpha\mu})$. The threshold of stability, and also the criterion that we used to construct the Arnold tongues, is when both equilibrium points coincide. So, we have that

$$\begin{aligned} & \phi_f^s = \phi_f^u \\ \Leftrightarrow\ & \pi - \arctan\left(\frac{\pi h^2 \epsilon}{4\alpha\mu}\right) = \arctan\left(\frac{\pi h^2 \epsilon}{4\alpha\mu}\right) \\ \Leftrightarrow\ & \arcsin\left(\frac{\pi h^2 \epsilon}{4\alpha\mu}\right) = \frac{\pi}{2} \\ \Leftrightarrow\ & \sin\left(\frac{\pi h^2 \epsilon}{4\alpha\mu}\right) = 1 \\ \Leftrightarrow\ & \frac{\pi h^2 \epsilon}{4\alpha\mu} = 1 \\ \Leftrightarrow\ & \alpha_t = \frac{h^2}{2\mu}\epsilon, \end{aligned} \tag{4.25}$$

which implies that, when we increase the effect of the dry friction, the value of α that marks this stability threshold, α_t, decreases. For this reason, the slope of the Arnold tongues, for each order of synchronization, is smaller for a higher value of μ. This is valid near the origin, that is, for small α and δ, since the relation $\phi_f^s = \phi_f^u$ (4.25) is based on the first order approximation values ϕ_f^s and ϕ_f^u computed by [23].

In figure 4.10 we observe that a higher value of μ provides a larger width to the Arnold tongues, at least within what is considered the valid physical context in terms of heigh. The effect of the friction, through this analysis, is to increase the stability of the system, becoming easier for both clocks to synchronize.

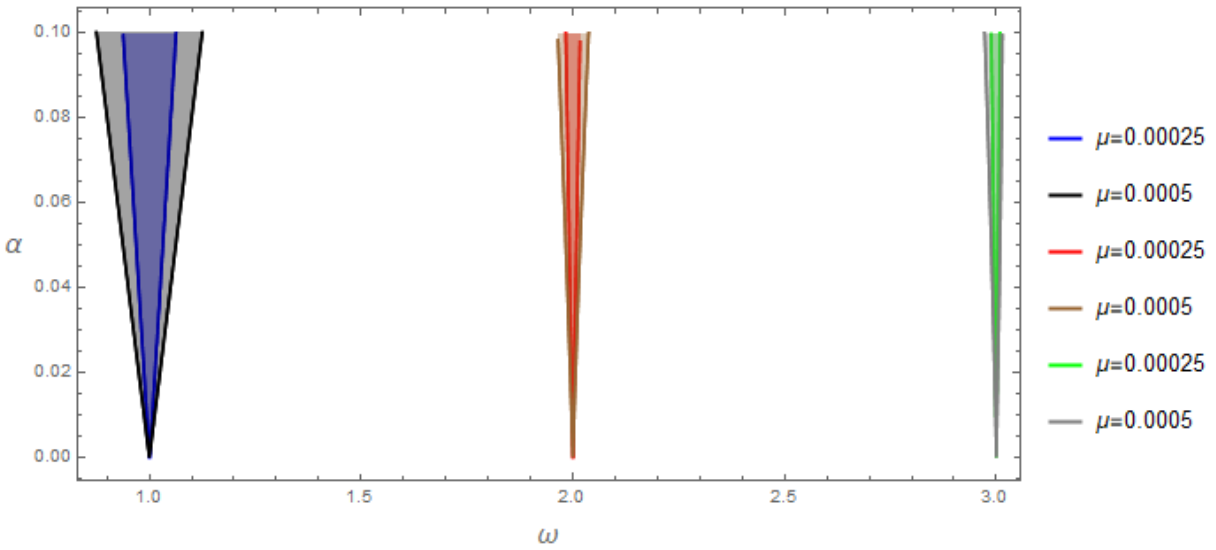

Figure 4.10: Comparison of Arnold tongues for different values of dry friction. We chose the values $\mu = 0.00025$ ($1:1$ (blue), $2:1$ (red) and $3:1$ (green)) and $\mu = 0.0005$ ($1:1$ (black), $2:1$ (brown) and $3:1$ (gray)) the adequate ones to compare the width at half height.The dashed line, still represents the limit value of α of the valid physical context (all values of μ are given in $m\ s^{-2}$).

5 A *KAM* like Theory for the Stability of Closed Orbits

The results presented in this section are new.

Kolmogorov-Arnold-Moser (KAM) theory deals with the persistence of quasi-periodic motions under a certain perturbation and was originally formulated by A. N. Kolmogorov in 1954, as an alternative approach to the perturbation theory to study the stability of near-integrable systems. The aim of this theory is to find approximate solutions of nonlinear problems such as the three body problem. The general result is achieved through linearizing the problem about an approximate solution, solving the linearized problem and improve the solution inductively [32].

Because our system is sectionally integrable, we can obtain explicitly the Poincaré map and, consequently, the same type of theory, allowing us to apply very similar results to those seen in [7, 32, 11].

In the coupled pendulum clocks, the impulse received by one of the clocks every time it passes through the vertical position represents a perturbation α in the system. There are two effects of this mutual perturbation to consider: one regards the phase difference, and its study leads to the phase locking discussed in [23]; the other is in the amplitude of the closed orbits in phase space.

In [23], the study that concerns the perturbation in the amplitude was not discussed thoroughly enough, however, it was stated that the system remains stable when the amplitude of the perturbations are very small in each cycle.

Yet, the study of the perturbed Poincaré map leads to a KAM like theorem for two coupled oscillators. The perturbed orbits in phase space remain in an appropriate neighborhood of the original torus – we see in this section how that happens: we did linearized the problem of the pendulum clock in the previous sections, but now it is our interest to increase the accuracy of the region in phase space to which the effect of the perturbation to the system extends. We do that by induction.

The impulse received by each clock perturbs the other at each cycle. This impulse, as we have already seen, in section 3, adjusts the final effective frequencies of each clock. What effect does it then produce in the amplitudes of each oscillator?

If the impulse is given at the same phase difference between both clocks, it corresponds to a slight change in the fixed point, as we have seen in the amplitude analysis of section 3.1. However, if we do not assume the existence of phase locking, the perturbation will depend strongly on the phase difference (now variable) at which the perturbation will occur. For instance, at the moment $C1$ receives its impulse, if the phase of $C2$ is π, its velocity will have an increment of $-\alpha$, its position will remain unchanged

and the radius of its limit cycle will suffer an increment of α. However, at that same instant, if the phase difference is $\frac{\pi}{2}$, the change in the velocity will be the same (an equal increment of α), although the effect on the radius will be negligible. With a zero phase difference, its radius will be decreased by $-\alpha$. The effect of the mutual perturbation will depend strongly on the relative position of the two oscillators.

Instead of writing explicitly this dependence on the perturbation in the phase difference at the beginning of each cycle of $C1$, we use an expedient that simplifies the problem without loss of generality: we consider that each one of the clocks has an impact on the other, producing a small bounded variation γ on the radius. This parameter depends on the phase difference of the clocks, which depends on the initial phase difference and n. We then have

$$-\alpha \leq \gamma(n) \leq \alpha. \tag{5.1}$$

Consequently, the previous fixed point in each cycle ceases to be constant and becomes affected by γ. Then, the new fixed point lies between

$$\frac{(A+\alpha)^2+h^2}{2(A+\alpha)} \text{ and } \frac{(A-\alpha)^2+h^2}{2(A-\alpha)}. \tag{5.2}$$

We do not know exactly the new actual map f_γ that governs the iteration of $C1$ (a similar map g_γ will act on $C2$). We know that this map depends on the variable γ. The iteration on the Poincaré section of $C1$ is given by

$$x_{n+1}^I = f_{\gamma(n)}\left(x_n^I\right), \tag{5.3}$$

analogously for $C2$,

$$x_{n+1}^{II} = g_{\gamma(n)}\left(x_n^{II}\right). \tag{5.4}$$

We assume that f has the form

$$f_{\gamma(n)}\left(x_n\right) = \sqrt{\left(x_n - A + \gamma\left(n\right)\right)^2 + h^2}, \tag{5.5}$$

$\forall_{n\geq 0}\, \forall_{x\geq A-\alpha}$, which has a small extra term inside the square root compared with the original Poincaré maps for the isolated oscillators, $f\left(x_n\right) = \sqrt{\left(x_n - A\right)^2 + h^2}$. Naturally, we have two strictly increasing functions

$$M\left(x\right) = f_\alpha\left(x\right) = \sqrt{(x - A + \alpha)^2 + h^2} \tag{5.6}$$

and

$$m\left(x\right) = f_{-\alpha}\left(x\right) = \sqrt{(x - A - \alpha)^2 + h^2}. \tag{5.7}$$

Both M and m satisfy the fixed point theorem, that is,

$$\lim_{n\to+\infty} M(x) = \frac{(A-\alpha)^2+h^2}{2(A-\alpha)} \tag{5.8}$$

and

$$\lim_{n\to+\infty} m(x) = \frac{(A+\alpha)^2+h^2}{2(A+\alpha)}. \tag{5.9}$$

We consider only the study of clock $C1$, once the study of $C2$ is similar. The orbit on the Poincaré section of $C1$ is denoted by

$$\left\{x_n\right\}_{n=0,1,2,\ldots} \tag{5.10}$$

We drop the superscript I for the sake of notational simplicity. We will not try to explicit the family $f_{\gamma(n)} = f_n$ of functions $f_n : \mathbb{R}^+ \to \mathbb{R}^+$. We consider only the fact

$$m\left(x\right) \leq f_n\left(x\right) \leq M\left(x\right), \ \forall_{n\geq 0}, \ \forall_{x\geq A-\alpha}. \tag{5.11}$$

We will not consider initial conditions less than $A - \alpha$. Therefore, we do not particularize what happens with f_n for $x < A - \alpha$.

The process of iteration on the right starts for initial conditions $x_0 > \frac{(A-\alpha)^2+h^2}{2(A-\alpha)}$. Considering, in terms of notation, x_n as the n-th iterated function f_n and y_n as the n-th iterated function M, and considering also the initial condition $x_0 = y_0$, by equation 5.11, we write

$$x_1 = f_0\left(x_0\right) \leq M\left(x_0\right) = y_1. \tag{5.12}$$

Consequently, in the next iteration, by equation 5.12 plus the strictly increasing property of M, we have

$$x_2 = f_1\left(x_1\right) \leq M\left(x_1\right) \leq M\left(y_1\right) = y_2, \tag{5.13}$$

and, by induction, we see that

$$x_{n+1} = f_n\left(x_n\right) \leq M\left(x_n\right) \leq M\left(y_n\right) = y_{n+1}. \tag{5.14}$$

Therefore, and because f_n is a family of functions, we apply the superior limit of iterations at both sides of 5.14. We get

$$\limsup_{n\to+\infty} f_n(x_n) \leq \limsup_{n\to+\infty} M(y_n). \tag{5.15}$$

The superior limit of M is the same as its limit. By 5.8, we write

$$\limsup_{n\to+\infty} x_{n+1} \leq \frac{(A-\alpha)^2 + h^2}{2(A-\alpha)}. \tag{5.16}$$

Now, using the notation $'$ to symbolize the iterations on the left, the process of iteration starts at the initial condition $x'_0 < \frac{(A+\alpha)^2+h^2}{2(A+\alpha)}$. Considering $x'_0 = y'_0$, once again, by equation 5.11, we have

$$m(x'_0) \leq f_0(x'_0). \tag{5.17}$$

By the same arguments stated from 5.12 to 5.14, is true that

$$y'_{n+1} = m(y'_n) \leq m\left(x'_n\right) \leq f_n\left(x'_n\right) = x'_{n+1}. \tag{5.18}$$

Now we apply the inferior limit of both members of the previous inequality, that is,

$$\liminf_{n\to+\infty} m(y'_n) \leq \liminf_{n\to+\infty} x'_{n+1}, \tag{5.19}$$

and once again, by 5.9, we have

$$\frac{(A+\alpha)^2 + h^2}{2(A+\alpha)} \leq \liminf_{n\to+\infty} x'_{n+1}. \tag{5.20}$$

Finally, it is known that

$$\liminf_{n\to+\infty} f_n(x_n) \leq \limsup_{n\to+\infty} f_n(x_n). \tag{5.21}$$

So, considering equation 5.21, from equations 5.16 and 5.20, we know that, from a certain order of iterations $n > k$, x_n becomes confined to a certain interval, i.e.,

$$\exists k \in \mathbb{N} : \forall n > k,\ \forall \delta > 0,$$
$$x_n \in \left]\frac{(A+\alpha)^2+h^2}{2(A+\alpha)} - \delta, \frac{(A-\alpha)^2+h^2}{2(A-\alpha)} + \delta\right[, \tag{5.22}$$

as we wanted to show. The associated Poincaré map is therefore represented by a band delimited by the dynamics of m and M, as shown in figure 5.1. This means that, under the Andronov model, the coupling of two isolated clocks corresponds to making a perturbation to the original torus in phase space, causing it to change to a blurred torus domain with dimensio 4.

The trajectories governed by the dynamics of f_n lie in the neighborhood of the original trajectories, so, the 4-dimensional blurred torus will also be in the neighborhood of the original one. The structure of the torus remains the same, meaning that under a perturbation γ in the conditions previously discussed, the system of two coupled clocks does not lose its stability.

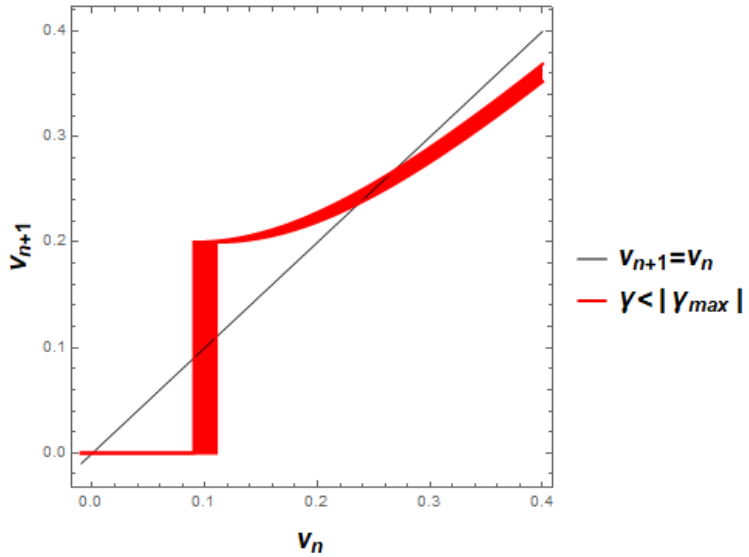

Figure 5.1: The red area is delimited by upper and lower functions m and M,respectively, and its interior corresponds to all the possible points of f_n. After a number $n > k$ of iterations, all the values of f_n will lie within $\left]\frac{(A+\alpha)^2+h^2}{2(A+\alpha)} - \delta, \frac{(A+\alpha)^2+h^2}{2(A+\alpha)} + \delta\right[$.

6 Possible Applications

Our work is based on a fundamental mathematical model, the Andronov model for an oscillator with impulses [3] and the synchronization is obtained by small discrete impacts. Thus, in principle, our methods can be applied to a multitude of physical systems. For the analysis of the possible applications of our study, however, we must distinguish two apparently similar but opposite system categories.

We make the distinction between a system of N *integrate and fire* oscillators [27, 19, 21, 8] and a system of N *damping and charge* oscillators. The former corresponds to a type of oscillator whose cycle is continuously charging until a threshold is reached; when this threshold is reached, a sudden discharge occurs, reseting the system onto its beginning and perturbing all the other oscillators in the system. The latter corresponds to a type of oscillator whose cycle is continuously losing energy (the damping) and when its phase reaches a critical value $\mod(2\pi)$, it is instantaneously charged. By *charge*, we are referring to as the potential energy of the system, which can be manifested in several forms – oscillating variables. In figure 6.1 we see the evolution of the oscillating variable with time in each of both types of oscillatory systems.

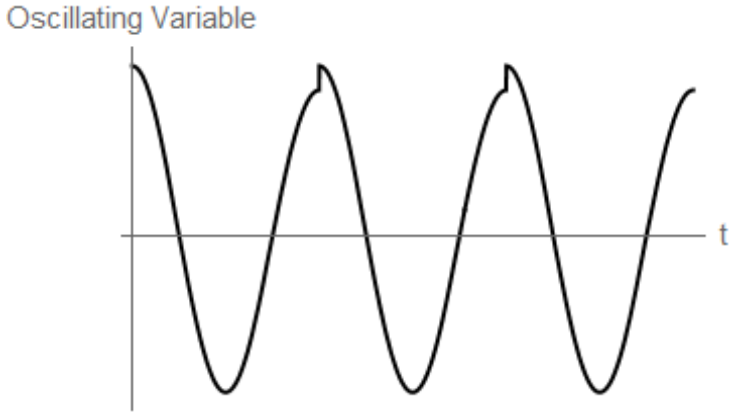

(a) Damping and charge oscillator.

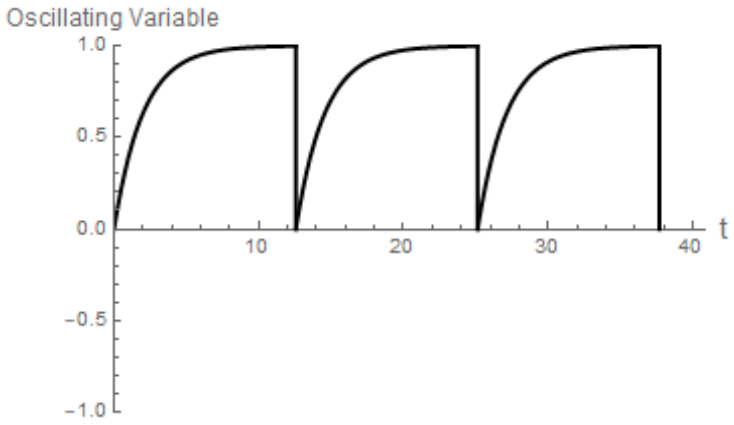

(b) Integrate and fire oscillator.

Figure 6.1: Different types of pulsed oscillators. We see that the intensity of the charge of that in subfigure is of much lower intensity than the discharge of the oscillator in subfigure .

We see here that there are some main differences between these type of oscillators that we can account: a) while integrate and fire oscillators have a continuous charging process and a punctual discharging process, damping and charge oscillators have a continuous discharging process and a punctual charging process; b) the sudden discharge of integrate and fire oscillators reset the system, they lead the system to zero charge (or potential energy). Damping and charge oscillators do not reset their charge, but instead, always increment the same amount of energy, so they adjust their charge to a certain value after a certain number of cycles. This value of charge is stable if the system returns to that value after some perturbation; c) while the period of integrate and fire oscillators depend on the time it takes to reach the

threshold, the period of the damping and charge depend exclusively on the time it takes for the phase to complete 2π, so it does not depend on the amount of energy within the system.

Point a) is a direct consequence of the fact that integrate and fire oscillators have a continuous source of external energy and damping and charge oscillators have a discrete source of external energy. In addition, the former have a discontinuous discharging process and the damping and charge oscillators have a continuous discharging process. Point b) is responsible for the fact that charges in damping and charge oscillators are always less intense than the discharges of the integrate and fire oscillators. This is a very important aspect, because although they are different processes, both the charge and the discharge are the processes responsible for the interaction among next neighbors. Therefore, because the interaction is weaker in the former, it is more difficult to find a stable equilibrium state for the dynamics of this case than for the dynamics of integrate and fire oscillators. The latter resets the charge of the oscillator, regardless of the amount of energy that it accumulates at every cycle. Points b) and c) explain why the integrate and fire oscillators constitute systems much more likely to synchronize than the ones constituted by damping and charge oscillators: firstly, because the cycle of the former allows a stronger intensity of interaction and secondly, because the interaction received by others always accelerates the charging process. In fact, for two coupled integrate and fire oscillators, Peskin [26] conjectured that (1) For arbitrary initial conditions, the system approaches a state in which all the oscillators are firing synchronously and that (2) this remains true even when the oscillators are not quite identical. Also, this conjecture was mentioned in the work of [21], where a more general version of Peskin's model was studied and analyzed for all N oscillators. In what concerns the damping and charge oscillators, not only the intensity is lower, as it may affect the phase of the next neighbors in both directions, in a sense that it may accelerate or delay their cycles.

This distinction is very important, since it provides us a clearer view over what are the main possible applications of our work. In fact, our Andronov clock is included in the category of a damping and charge oscillator, because of its periodic external force and its continuous damping. Intuitively, we see that it corresponds to case a) of figure 6.1. We encounter many documented and well known integrate and fire like systems. Fireflies [21, 29], neuronal activity and epileptic episodes [31, 12] and cardiac pacemakers [26, 25], are some good examples, among many others. Thus, using the Andronov model to describe damping and charge like systems, which are less known, is a great challenge for us. However, systems like coupled pendulum clocks are a good example of applications.

What we can do, also, is to compare the results of both models. We are referring to characteristics such as time spent since the beginning of the interaction until the phase locking, the relaxation time and even the duration of transient synchronization states.

There are several applications within the context of pulsed oscillators – where we include both the integrate and fire and the damping and charge oscillators –, namely in the domain of electronics and biology. Relatively to the former, our application of the Andronov model for an oscillator with impulses can be generalized for two coupled electronic signals. For instance, two 555 timer integrated circuits, one of the most common electronic timer devices, also used as the common computer clock, connected in parallel with the same source share a week interaction between them: every time the signal changes from state 0 to state 1 or *vice versa*, that change of state perturbs slightly the value of the voltage of the other oscillator, consequently slowing down or accelerating the time period of stay of the other oscillator in one of the two possible states. This sequence of perturbations from each clock to another, may lead them to adjust their cycles, analogously to what happens with mechanical pendulums. This is a physical system to which the Andronov model might be applicable: although each electronic oscillator acts like a capacitor – being, therefore, of an integrate and fire oscillator type –, a system of two coupled electronic clocks may be described by two oscillatory systems that interact throught localized weak impulses, as in our model of the coupled clocks.

In this particular case, these clocks may synchronize with a zero phase difference or in phase opposition, according to lab experiments performed by the same authors of [23], but with the respective results not yet published.

Regarding the realm of biology, as mentioned in section 1.1, several species can exhibit synchronous behavior as, for instance, fireflies [27, 29] or flocking birds [9]. Relatively to the former, in a population of fireflies, each individual produces a flash of light periodically. The light dynamics throughout the entire population is achieved through a initial and local communication between the nearest neighbors for each firefly. The initial delay in time response from one to others adjusts firstly to a local group time response average, then to the average of a larger group and so forth. The limit, of course, is the average of the ultimate group, the entire population. Once phase locking is achieved, every firefly flashes in unison with the others. There are many models with this type of interaction but the actual mechanism is not completely understood.

One of the models applied to this system is the Kuramoto model for synchronization of oscillators, since it is of integrate and fire type, and whose techique is explained briefly in subsection 1.2. It involves perturbative methods, which we did not intend to develop in this dissertation. However, simulations could be made for the dynamics of a population of light emitters that would follow the properties of an Andronov clock. For instance, a firefly with a certain light emission intensity that would gradually decrease in a time period. At the end of its cycle, an internal stimulus would increase the light intensity, and so forth. In this case, our work would be to establish a network of entities with the same properties and develop our model to N coupled oscillators within this framework. The contrast to the Kuramoto model should be made, for instance, when comparing time of synchronization and of relaxation for both models.

Still in the realm of biology, neuronal activity is one of the main subjects inherent to the study of synchronization and there is plenty of documentation on this subject. One of the main studies on this matter is *anticipated synchronization* in neuronal motifs and networks. Anticipated synchronization is a form of synchronization that occurs when a unidirectional influence is transmitted from an emitter to a receiver, but the receiver system leads the emitter in time [20]. Both the receiver and the emitter systems are connected by a synapse. The synapse is the channel responsible to transmit electrochemical waves from one neuronal group to another, through the variations of ion concentration along it. In the context of our work, the emitter and the receiver correspond, respectively, to the master and the slave oscillators. Also, in the work of [20], which is based on the original work of Voss [31], each oscillator corresponds to a group of neurons, and not to a single one. What happens is that, although each neuron may be considered as a solo oscillator, it follows the oscillation of the average frequency of its group. Therefore, the study approach of the anticipated synchronization is concerned to one neuronal group as a whole. The main difference in the work of Voss is that there is a continuous external power supply whereas in our work we consider a discrete succession of external impulses. This is a fundamental matter. Nonetheless, with further studies, our model may be adapted to this problem.

As said, anticipated synchronization is one of the very well documented phenomena of many that happen in the brain. The reason why this is such a relevant problem is, for instance, the prevention of sudden epileptic seizures, that affect a part of the population. An epileptic seizure is a transient occurrence of signs and/or symptoms due to abnormal excessive or synchronous neuronal activity in the brain [12]. So, what we expect with the development of the study on synchronization is actually to help preventing it, in this case. A notorious example of an evidence of the desynchronization phenomenon in the brain and its consequence is documented in [13]. Here, it was shown that when a single long bar of optimal orientation, velocity and preferred direction passed through the receptive field of recorded neurons in the primary visual cortex of anesthesized cat, a synchronous activity with an average frequency of $40Hz$ was observed. When two separate and smaller bars in the same conditions passed through the cat's visual field, there was a decrease in the synchrony between the neural responses to the separate bars. This remarkable result, among others in this particular work, suggests that there is a correlation between firing times of neurons and different objects presented (other results were shown that support this conclusion). This has no intervention of any recognition activity whatsoever, since the animals used in these experiments were unconscious. Therefore, the application of our study on the phenomenon of desynchronization plays an important role as well.

7 Conclusions

We review the literature in subsections 1.2,1.3,2.1 and 3.1 and present new results in subsections 3.2, 4.1, 4.2, 4.3 and section 5.

To summarize, in subsection 2.1 we introduced the Andronov model for an oscillator with impulses and applied it to a pendulum clock, once this physical system is under the conditions established by the model. This system falls into the category of a *damping and charge* oscillator, in opposition to an *integrate and fire* oscillator.

We first made a study on the amplitude of oscillations. We observed that the Poincaré Map for the velocity has an attractive fixed point, which is associated, in consequence, to an attractive closed orbit. Therefore, we conclude that the sequence of oscillations tends to stabilize at the value of velocity $v = \frac{2\mu}{\omega} + \frac{\omega h^2}{8\mu}$.

In section 3.1 we analysed the system of two coupled Andronov clocks with a frequency relation of $1:1$. We first made a study on the amplitude evolution of one clock. We considered that the coupling with its pair involves a perturbation on the amplitude of its limit cycle. We found a stable fixed point for the velocity of the system, which is

$$v^* = \frac{(A+\alpha)^2 + h^2}{2(A+\alpha)}, \qquad A = 4\mu/\omega, \tag{7.1}$$

where A is the dry friction component and α is the perturbation generated by the escapement of the other clock.

In a phase analysis, we mapped the phase difference between both clocks along the cycles. The values found for the stable and unstable fixed points of these maps, in first order approximation were, respectively, $\phi_f^s = \pi + \arcsin\left(\frac{\pi h^2 \delta}{8\alpha\mu}\right)$ and $\phi_f^u = -\arcsin\left(\frac{\pi h^2 \delta}{8\alpha\mu}\right)$. Therefore, for very similar frequencies, that is, when $\epsilon << 1$, then $\phi_f^s \approx \pi$ and $\phi_f^u \approx 0$. This means that two Andronov clocks with near frequencies tend to synchronize in phase opposition, where the phase is scaled to the slowest clock.

In subsection 3.2 we studied the evolution of the phase difference of the two coupled Andronov clocks, but now with a frequency relation of $2:1$. The maps of the phase difference exhibit two equilibrium points, one stable and another unstable, which are respectively, $\phi_f^s = \pi + \arcsin\left(\frac{\pi h^2 \delta}{2\alpha\mu}\right)$ and $\phi_f^u = -\arcsin\left(\frac{\pi h^2 \delta}{2\alpha\mu}\right)$. Once again, for similar frequencies, $\epsilon << 1$, we have $\phi_f^s \approx \pi$ and $\phi_f^u \approx 0$. Both clocks still synchronize in phase opposition.

In subsection 4.1, we constructed the linear expansions of the original nonlinear maps through the phase approximation method. We observe that they exhibit the same behavior as the nonlinear map composition, near $\alpha = 0$ and $\epsilon = 0$. We generalize this expansion for every frequency relation, $N:1$. Furthermore, we observed a symmetry-type feature for the case $N = 1$. For $N > 1$ we observed that the influence of the fastest clock over the other loses relevance, meaning that with the increase of N, there is a tendency to a *master-slave* behavior: the slowest clock dictates the rhythm of synchronization. We then conjectured the following:

Conjecture:
The relation between two Andronov clocks for $N:1$, where $N > 1$, with an interaction of the same type, that is, $\pm\alpha$, is always master-slave.

We leave this conjecture to be demonstrated in a future work.

In section 4.2 we expand the composition of maps for the case $1:1$ until the second order, around $\alpha = 0$ and $\epsilon = 0$. It has an even more according behavior with the nonlinear map $1:1$ than its first order expansion, as we can verify graphically. Here we verify the match between the original dynamics, the first order approximation, obtained by phase approximation construction and the second order approximation, reinforcing the results.

In subsection 4.3 we construct the regions of synchronization in the parameter space (ϵ, α) – the

Arnold Tongues –, for the first, second and third orders of synchronization. The higher the order of synchronization, the thinner is the Arnold tongue. This means that, due to the increasing nonlinearity with N, for each value of α the window of possible values ϵ that enable the conditions for synchronization is smaller. We also do this analysis for values of $\alpha > h$, where h is the correspondent to the kinetic energy provided by the escapement, according to the conditions of the problem.

Still in this section, we observe a graphic visual match between the Arnold tongues constructed from the original map compositions and the respective linear first order expansions, with very positive results.

When we look to the effect of the dry friction, we observe that the higher the value of the friction, the larger the width of each Arnold tongue. This is due to the importance that the perturbation α gets with the increase of μ, that is, for a higher μ, we do not need such a high value of α to enter in a synchronization region of the parameter space.

In the last section, 5, instead of describing the problem in a deterministic perspective, we did not assume that phase locking could occur. Therefore, the intensity of the perturbation depends on the phase difference between both clocks. The previous perturbation, treated in the previous sections, was now considered to be stochastic.

The system of two coupled clocks can be seen in phase space as surface of a 2-dimensional torus, as a result from the product of their respective limit cycles. We showed that, under a stochastic perturbation (bounded and limited), using the fixed point theorem, the new fixed points still remain in a neighborhood of each other. In consequence, their respective orbits in the phase space, likewise. Thus, the perturbed system, which can be represented by a 4-dimensional blurred torus in the phase space, lies in a neighborhood of the original 2D-torus. This is a proof that the system of two coupled Andronov clocks is structurally stable.

8 Future work

For the continuation of this work, we intend to carry out experiments with the same pendulum clocks used in the work of [23], using, still, the Andronov model to compare theoretical with experimental results. Variations of the experiment, such as the distance between the clocks, the value of the dry friction from the escapement and the material considered for the beam must be made in order to change, respectively, the time for synchronization, the dissipation of energy and the effect of the perturbation in the other clock. These are primary examples that we can test to consolidate the theoretical results.

Also, experiments must be done with other type of oscillators. A good and achievable example are electronic oscillators. The purpose here is to couple two computer clock signals connected in parallel and proceed with the same steps as we did with the pendulum clocks. In this case, however, we expect different values for the fixed points than the ones for the pendulum clocks. Also, the type of interaction is different than the one we deal with in this work.

Afterwards, we intend to use the same model to predict the behavior and the points of stability of 3 oscillators coupled in line. Here, the approach is based on a generalization of the Andronov model, since we apply the method used in this work to N Andronov oscillators. This problem may reduced to $N-1$ systems of 2 oscillators (considering the constraints of the next neighbors' interactions), whose results we are already familiarized with. Some unexplored aspects in this thesis work must be taken into account, but the problem of N oscillators in a line arrangement should be easy to treat. This generalization should work also for a set of electronic oscillators, although this case is more delicate, since the basis of the problem of electronic circuits is slightly different from the one of the mechanical clocks. After an in-depth study of just one solo electronic oscillator and two coupled ones and after we adapt the Andronov model to these cases, our goal is to study 3 coupled oscillators in line and then generalize the model for N oscillators.

Moreover, we intend to apply, as far as possible, the Andronov model to a system of oscillators in a triangle configuration. Of course, this is a 3 body problem, which implies a much more complex analysis than a linear problem such as the one for N oscillators in line. More interactions must be taken into account, as well as the type of interaction and its intensity. It is possible that our approach requires a different base model to study dynamics of this system in detail. Of course, this is considering identical oscillators. Once we are able to predict the behavior of 3 physical oscillators in such conditions, we should find the analogous arrangement for electronic oscillators, which is not obvious at all.

Our study might also be applied to molecular oscillators. Molecular systems are very complex systems and, since the measurement techniques are very restrictive in terms of accuracy, a base model like Andronov's must be applied to, at most, two molecular oscillators. Of course, when we refer to molecular oscillators, we include groups of oscillators that pulse in unison. A stricking example of that is the one studied in [20], where a population of neurons in the cortex is considered to be a whole oscillator. Oscillating neuron populations are connected through synapses, creating, in this way, a network constituted by nodes (neuron populations) and links (synapses). This particular example is based on the work [31], where *anticipated synchronization* is mentioned for the first time. In [31], a different base model is used to explain the phenomena of anticipated synchronization, so our goal is to obtain conclusions – preferably the same conclusions – on the same biological system as the one addressed in [20], but using the Andronov model for an oscillator with impulses, with the appropriate amendments.

In all of these levels of the development of our study must be included the time of synchronization of the oscillators involved in each system. Not every physical system synchronizes and, the ones that do so, might take a while. Synchronization state may be just a transitory state. We intend to calculate the time that takes to reach synchronization and how long the system holds up into that state. This is the case of the epileptic seizures. Predicting the duration of this transitory state is important to, in some manner, help comprehending the development of the phenomena in the brain tissue. Of course, this is a wider scale than the one addressed by the work [20] and involves a higher number of self-sustained oscillators, but still it has its importance and its applicability. Another example of the importance of the time for synchronization is in electronic coupled oscillators. This calculation may help predict the error of electronic signal transmission.

Finally, we intend to demonstrate the conjecture exposed in section 4.1.

Within this framework, we expect to continue the development of the study of synchronization of physical oscillators as soon as possible, having already a strategy of research, with experimental goals in mind to accomplish.

References

[1] Ralph Abraham and Alan Garfinkel. The dynamics of synchronization and phase regulation. *Preprint, MS*, 111, 2003.

[2] Robert Adler. A study of locking phenomena in oscillators. *Proceedings of the IRE*, 34(6):351–357, 1946.

[3] Aleksandr A Andronov, Aleksandr A Vitt, and Semen E Khaikin. *Theory of Oscillators: Adiwes International Series in Physics*, volume 4. Elsevier, 2013.

[4] Gregory L Baker and James A Blackburn. *The Pendulum: a case study in physics*. Oxford University Press, 2005.

[5] Matthew Bennett, Michael F Schatz, Heidi Rockwood, and Kurt Wiesenfeld. Huygens's clocks. *Proceedings: Mathematics, Physical and Engineering Sciences*, pages 563–579, 2002.

[6] James A Blackburn, Niels Gro/nbech-Jensen, and H J T Smith. Harmonic synchronization in resistively coupled josephson junctions. *Journal of applied physics*, 75(7):3668–3673, 1994.

[7] Henk W Broer and Mikhail B Sevryuk. KAM theory: Quasi-periodicity in dynamical systems. *Handbook of Dynamical Systems*, 3:249–344, 2010.

[8] Shannon R Campbell, DeLiang L Wang, and Ciriyam Jayaprakash. Synchrony and desynchrony in integrate-and-fire oscillators. *Neural computation*, 11(7):1595–1619, 1999.

[9] J Michael Davis. The coordinated aerobatics of dunlin flocks. *Animal Behaviour*, 28(3):668–673, 1980.

[10] Gregory C Dente, Charles E Moeller, and Peter S Durkin. Coupled oscillators at a distance: Applications to coupled semiconductor lasers. *IEEE journal of quantum electronics*, 26(6):1014–1022, 1990.

[11] H Scott Dumas. *The KAM Story: A Friendly Introduction to the Content, History, and Significance of Classical Kolmogorovâ Arnoldâ Moser Theory*. World Scientific Publishing Company, 2014.

[12] Robert S Fisher, Walter van Emde Boas, Warren Blume, Christian Elger, Pierre Genton, Phillip Lee, and Jerome Engel. Epileptic seizures and epilepsy: Definitions proposed by the international league against epilepsy (ilae) and the international bureau for epilepsy (ibe). *Epilepsia*, 46(4):470–472, 2005.

[13] Charles M Gray, Peter König, Andreas K Engel, and Wolf Singer. Oscillatory responses in cat visual cortex exhibit inter-columnar synchronization which reflects global stimulus properties. *Nature*, 338(6213):334, 1989.

[14] John Guckenheimer and Philip Holmes. *Nonlinear Oscillations, Dynamical Systems, and Bifurcations of Vector Fields*, volume 42. Springer Science & Business Media, 2013.

[15] Andrey Gushchin, Enrique Mallada, and Ao Tang. Phase-coupled oscillators with plastic coupling: Synchronization and stability. *IEEE Transactions on Network Science and Engineering*, 3(4):240–256, 2016.

[16] Morris W Hirsch, Stephen Smale, and Robert L Devaney. *Differential Equations, Dynamical Systems, and an Introduction to Chaos*. Academic press, 2012.

[17] Christiaan Huygens. Letters to de sluse,(letters; no. 1333 of 24 february 1665, no. 1335 of 26 february 1665, no. 1345 of 6 march 1665), 1895.

[18] Shyam K Joshi, Shaunak Sen, and Indra N Kar. Synchronization of coupled oscillator dynamics. *IFAC-PapersOnLine*, 49(1):320–325, 2016.

[19] Yoshiki Kuramoto. Cooperative dynamics of oscillator community: a study based on lattice of rings. *Progress of Theoretical Physics Supplement*, 79:223–240, 1984.

[20] Fernanda S Matias. *Anticipated synchronization in neuronal circuits*. PhD thesis, Universidade Federal de Pernambuco.

[21] Renato E Mirollo and Steven H Strogatz. Synchronization of pulse-coupled biological oscillators. *SIAM Journal on Applied Mathematics*, 50(6):1645–1662, 1990.

[22] Ana M Nunes and José V Pereira. Phase-locking of two andronov clocks with a general interaction. *Physics Letters A*, 107(8):362–366, 1985.

[23] Henrique M Oliveira and Luís V Melo. Huygens synchronization of two clocks. *Scientific reports*, 5:11548, 2015.

[24] Jose V Pereira. A theorem on phase-locking in two interacting clocks (the huyghens effect). In *Dynamical Systems and Microphysics: Geometry and Mechanics*, pages 343–352. Elsevier, 1982.

[25] Charles S Peskin. Mathematical aspects of heart physiology. *Courant Inst. Math*, 1975.

[26] Charles S Peskin. Self-synchronization of the cardiac pacemaker. *Mathematical Aspects of Heart Physiology, New York University: New York*, pages 268–278, 1975.

[27] Arkady Pikovsky, Michael Rosenblum, and Jürgen Kurths. *Synchronization: a Universal Concept in Nonlinear Sciences*, volume 12. Cambridge university press, 2003.

[28] M Senator. Synchronization of two coupled escapement-driven pendulum clocks. *Journal of Sound and Vibration*, 291(3-5):566–603, 2006.

[29] Hugh M Smith. Synchronous flashing of fireflies. *Science*, 82(2120):151–152, 1935.

[30] Steven H Strogatz. *Nonlinear Dynamics And Chaos: With Applications To Physics, Biology, Chemistry, And Engineering*. CRC Press, 2018.

[31] Henning U Voss. Anticipating chaotic synchronization. *Physical review E*, 61(5):5115, 2000.

[32] C Eugene Wayne. An introduction to KAM theory. In *Dynamical Systems and Probabilistic Methods in Partial Differential Equations (Berkeley, CA, 1994)*, volume 31, pages 3–29. Amer. Math. Soc. Providence, RI, 1996.